



Early precursor T cells establish and propagate T cell exhaustion in chronic infection

Daniel T. Utzschneider^{ID 1,7}✉, Sarah S. Gabriel^{1,7}, David Chisanga^{ID 2,3,4,5}, Renee Gloury¹,
Patrick M. Gubser¹, Ajithkumar VasanthaKumar^{ID 1,3}, Wei Shi^{2,3,5,6} and Axel Kallies^{ID 1,3}✉

CD8⁺ T cells responding to chronic infections or tumors acquire an 'exhausted' state associated with elevated expression of inhibitory receptors, including PD-1, and impaired cytokine production. Exhausted T cells are continuously replenished by T cells with precursor characteristics that self-renew and depend on the transcription factor TCF1; however, their developmental requirements are poorly understood. In the present study, we demonstrate that high antigen load promoted the differentiation of precursor T cells, which acquired hallmarks of exhaustion within days of infection, whereas early effector cells retained poly-functional features. Early precursor T cells showed epigenetic imprinting characteristic of T cell receptor-dependent transcription factor binding and were restricted to the generation of cells displaying exhaustion characteristics. Transcription factors BACH2 and BATF were key regulators with opposing functions in the generation of early precursor T cells. Overall, we demonstrate that exhaustion manifests first in TCF1⁺ precursor T cells and is propagated subsequently to the pool of antigen-specific T cells.

CD8⁺ T cells responding to chronic infections or tumors differentiate into a dysfunctional state widely known as 'T cell exhaustion'. T cell exhaustion has been described in murine models of chronic lymphocytic choriomeningitis virus (LCMV) infection and in a variety of human chronic viral infections, including infections with the human immunodeficiency virus or hepatitis B and C viruses^{1–3}. Similarly, T cell exhaustion is a common feature of tumor-infiltrating T cells in both humans and mice^{4–6}. Exhausted T cells are characterized by elevated expression levels of inhibitory receptors such as PD-1, Lag-3, 2B4, TIM-3 and CD160, and a gradual loss of effector function including an impaired ability to secrete interferon- γ (IFN- γ) and tumor necrosis factor^{1,2,7,8}. Enhanced and persistent T cell receptor (TCR) stimulation is the main driver of T cell exhaustion^{1,2,9,10}. Consistent with this notion, various TCR-responsive transcription factors such as NFATC1, IRF4, BATF and TOX are expressed at elevated levels in exhausted T cells and contribute to the acquisition of their dysfunctional state^{11–17}. In particular, TOX has been identified as being specifically expressed in exhausted T cells and to have a crucial impact on their development and maintenance^{11,13–15}.

The pool of exhausted CD8⁺ T cells is heterogeneous, consisting of subsets with distinct functional properties and developmental potential. Multiple labs have identified a population of exhausted T cells that express molecules typically associated with memory T cells such as the transcription factor TCF1. In contrast to most exhausted T cells, TCF1⁺ cells lack expression of TIM-3, retain high proliferative potential and undergo long-term self-renewal, while also replenishing the dominant population of TCF1⁻ exhausted effector T cells^{8,18–22}. Thus, they serve as progenitors or 'precursors of exhausted' T (TPEX) cells and are therefore essential to perpetuate antigen-specific T cell responses over long periods^{1,2,7,8}. Importantly, despite exhibiting critical features of T cell exhaustion

such as high expression of TOX and PD-1, as well as an impaired ability to produce cytokines, TCF1⁺ TPEX cells in chronic infection retain the highest developmental potential among the exhausted T cell pool^{8,11–15,19,23,24}. Indeed, several studies have found that the therapeutic success of PD-1 and its ligand PD-L1 checkpoint inhibition relied on the proliferative fitness of TCF1⁺ TPEX cells^{19–21}, and their frequency positively correlated with the success of cancer immunotherapy^{25–28}.

Studies have further dissected the pool of exhausted T cells based on the expression of the chemokine receptor CX3CR1 (refs. ^{23,24}). TCF1⁻CX3CR1⁺ exhausted T cells are the immediate progeny of TCF1⁺ TPEX cells, maintain the highest effector function and are critical for mediating some level of control in chronic viral infections^{23,24}. Loss of CX3CR1 demarcates acquisition of a terminally exhausted state in which effector functions are strongly diminished^{23,24}. Thus, antigen-specific T cells in chronic infections display considerable heterogeneity and are maintained by intricate precursor and progeny relationships. However, the first nodes in the network that underpin chronic T cell responses, in particular the developmental requirements of TCF1⁺ TPEX cells, are still poorly understood, thus limiting the rational development of new immunotherapies.

In the present study, we demonstrate that TCF1⁺ precursor and TIM-3⁺ effector T cells arise early in response to acute and chronic viral infections. Unexpectedly, we find that high amounts of antigen promote the generation of precursor T cells. Early precursor T cells responding to chronic infection acquire transcriptional and epigenetic hallmarks of exhaustion within a few days, whereas early effector T cells resemble polyfunctional T cells found in response to acute infection. Furthermore, we reveal that the transcription factors BACH2 and BATF regulate the generation of early precursor and effector T cells in an opposing manner. Overall, we propose a

¹Department of Microbiology and Immunology, The Peter Doherty Institute for Infection and Immunity, University of Melbourne, Melbourne, Australia.

²Olivia Newton-John Cancer Research Institute, Heidelberg, Australia. ³The Walter and Eliza Hall Institute of Medical Research, Melbourne, Australia.

⁴Department of Medical Biology, University of Melbourne, Melbourne, Australia. ⁵School of Cancer Medicine, La Trobe University, Heidelberg, Victoria, Australia. ⁶School of Computing and Information Systems, University of Melbourne, Melbourne, Australia. ⁷These authors contributed equally:

Daniel T. Utzschneider, Sarah S. Gabriel. ✉e-mail: daniel.utzschneider@unimelb.edu.au; axel.kallies@unimelb.edu.au

model in which T cell exhaustion is first established in TCF1⁺ precursor T cells, and only subsequently disseminated to the pool of antigen-specific effector T cells through the replenishment of poly-functional effector cells with exhausted T cells.

Results

T cells differentiate into early precursor and effector cells. To track the development of TCF1⁺ precursor T cells, we transferred TCR transgenic CD8⁺ P14 T cells specific for the LCMV-derived gp33-41 epitope, labeled with a cell division tracker dye, into naive mice, which were then challenged with either LCMV Armstrong or Docile, which cause acute or chronic infections, respectively (see Extended Data Fig. 1a,b). After only three cell divisions, P14 T cells separated into TCF1⁺TIM-3⁻ precursor T (TP) cell and TCF1⁻TIM-3⁺ effector T (TE) cell subsets (Fig. 1a,b). Although this separation was independent of the type of infection, P14 T cells responding to LCMV Docile maintained two- to threefold higher frequencies of TCF1⁺ TP cells during the expansion phase of the infection (Fig. 1b–e)²⁹. This enhanced development of TCF1⁺ TP cells early during Docile infection was unexpected, because mice infected with LCMV Docile had much higher (~40-fold) viral titers than those infected with LCMV Armstrong (Fig. 1f), and increased TCR engagement is thought to promote the differentiation of effector cells at the expense of memory-fated cells³⁰. To investigate the relationship between viral titer and thus antigen burden and the development of TCF1⁺ TP cells, we infected mice with titrated doses of LCMV Docile. Consistent with our initial observation, increasing doses of virus resulted in the generation of larger frequencies of early TCF1⁺ TP cells (Fig. 1g), and there was a tight correlation between viral burden and the frequencies of TCF1⁺ TP cells (Fig. 1h). This was further validated using a previously described mixed chronic LCMV infection^{9,11} in which we specifically reduced the amount of LCMV-derived gp33 antigen while retaining a similar viral load and inflammation (Fig. 1i). Indeed, reducing the amount of antigen, while keeping the overall infection the same, resulted in a substantial reduction in TCF1⁺ TP cells (Fig. 1j,k). Thus, high amounts of antigen promote the differentiation of TP cells.

Reduced effector function of early TP cells. Next, we compared the acquisition of features of T cell exhaustion among early TP and TE cells responding to infections with acute or chronic LCMV strains. Within the first 3 days of infection, TP and TE cells responding to Docile or Armstrong infection upregulated expression of PD-1 and TOX (see Extended Data Fig. 1c,d). However, while in response to Docile infection TP and TE cells further increased expression levels of both molecules with ongoing cell divisions, it was transient in Armstrong infection (see Extended Data Fig. 1c,d). Thus, on day 5 post-infection, Docile-derived T cells expressed substantially higher levels of PD-1 and TOX compared with T cells in Armstrong-infected mice (see Extended Data Fig. 1e–g). Consistent with our finding that TP cells require strong TCR signals for their differentiation, day 5 TP cells in both infections expressed more TOX compared with their TE counterparts (Fig. 2a,b). However, this difference diminished over time in Docile infection (Fig. 2c). In both infections, day 5 TP cells produced lower quantities of IFN-γ compared with their TE cell counterparts, but the IFN-γ production in TP cells from Docile infection was substantially lower than that of TP cells from Armstrong infection (Fig. 2d,e). Interestingly, when we infected mice with titrated doses of Docile virus, we observed an enhanced ability of TP cells to produce IFN-γ with decreasing doses of virus (Fig. 2f). This was not observed for TE cells (Fig. 2g), indicating that increased levels of antigen not only favor early TP generation, but also specifically repress their effector function. TE cells from Docile-infected mice rapidly lost their ability to produce IFN-γ, whereas TP cells sustained low levels of cytokine production over time (Fig. 2h). As expected, after an

acutely resolved Armstrong infection, TOX expression was low and the cytokine-producing capacity of memory cells was very high compared with both exhausted TP and TE cells in chronic Docile infection (see Extended Data Fig. 2). Overall, these observations suggested that early TCF1⁺ precursor cells, and not effector cells, are the first to acquire features of T cell exhaustion during chronic infection.

ID3 demarcates precursor T cells in acute and chronic infection. To further examine TP cell differentiation and exhaustion, we took advantage of *Id3*^{GFP} reporter mice. Similar to established exhausted T cells and their precursors^{22,29}, day 5 TIM-3⁻ TP cells in both Armstrong and Docile infections expressed elevated amounts of ID3 whereas TIM-3⁺ TE cells lacked ID3 expression (Fig. 3a). Although ID3 was upregulated and maintained at high levels in TIM-3⁻ cells throughout chronic infection (Fig. 3a, top), ID3⁺ cells were less prominent in acute infection, and their frequencies remained low throughout the memory phase (Fig. 3a,b). In both infections, ID3⁺ cells co-expressed TCF1 and other well-known markers used to identify precursors of exhausted T cells in established chronic infections⁸ such as Ly108 (SLAMF6) and CXCR5 (Fig. 3c,d and see also Extended Data Fig. 3a–c), and lacked expression of molecules associated with effector and exhausted T cells, such as Granzyme B, 2B4 and CD39 (see Extended Data Fig. 3d). Thus, ID3 delineates precursor T cells in both acute and chronic infections. In contrast, TCF1 was more broadly expressed, including in ID3⁺ and ID3⁻ memory T cells after acute infection (Fig. 3e). In conclusion, the combination of ID3 and TIM-3 expression faithfully identified TP and TE cells in ongoing Docile and Armstrong infections and allowed for the delineation of a minor subset of memory T cells with characteristics similar to the precursors of exhausted T cells.

TP cells acquire transcriptional features of exhaustion first. Next, we sorted TP and TE cells using *Id3*^{GFP} reporter P14 T cells at different time points post-LCMV Docile and Armstrong infection and performed RNA-sequencing (RNA-seq). Analysis of the data revealed large numbers of genes differentially expressed (DE) between early (day 5) TP and TE cells in both Docile and Armstrong infections. This included genes involved in memory development such as *Tcf7* and *Bach2*, as well as genes implicated in effector differentiation and function including *Id2* and *Gzmb*, and exhaustion such as *Entpd1* (CD39) (Fig. 4a and Extended Data Fig. 4a and Extended Data Tables 1 and 2). Notably, these differences became more pronounced in Docile infection over time (Fig. 4b). In contrast, after viral clearance in Armstrong-infected mice, ID3⁺ and ID3⁻ T cells became more similar, which was in line with the development of both subsets into resting memory T cells (see Extended Data Fig. 4b,c and Extended Data Tables 3 and 4). Multi-dimensional scaling (MDS) analysis of all RNA-seq samples resulted in clustering of populations based on infection kinetics in dimension 1 ('Time') and type of infection in dimension 2 ('Exhaustion', Fig. 4c). Indeed, independent of the time post-infection, all TP cells from Docile-infected mice clustered in dimension 1 at the top (upper gray box), whereas fully exhausted TE cells from Docile-infected mice (days 12 and 21) clustered at the bottom of the plot (Fig. 4c, lower gray box). In contrast, all samples derived from acute infection clustered in the middle of the plot (Fig. 4c, green box). Notably, however, TE cells isolated early (day 5) from Docile-infected mice clustered closely with their effector counterparts derived from Armstrong-infected mice (Fig. 4c). Thus, early TP cells derived from Docile-infected mice transcriptionally resembled established precursors of exhausted T cells, whereas early TE cells from the same mice resembled polyfunctional effector cells derived from an acute Armstrong infection.

To identify subset-specific and common genes linked to differentiation of precursors of exhausted T cells and exhaustion, we identified DE genes between ID3⁺ and ID3⁻ exhausted T cells from

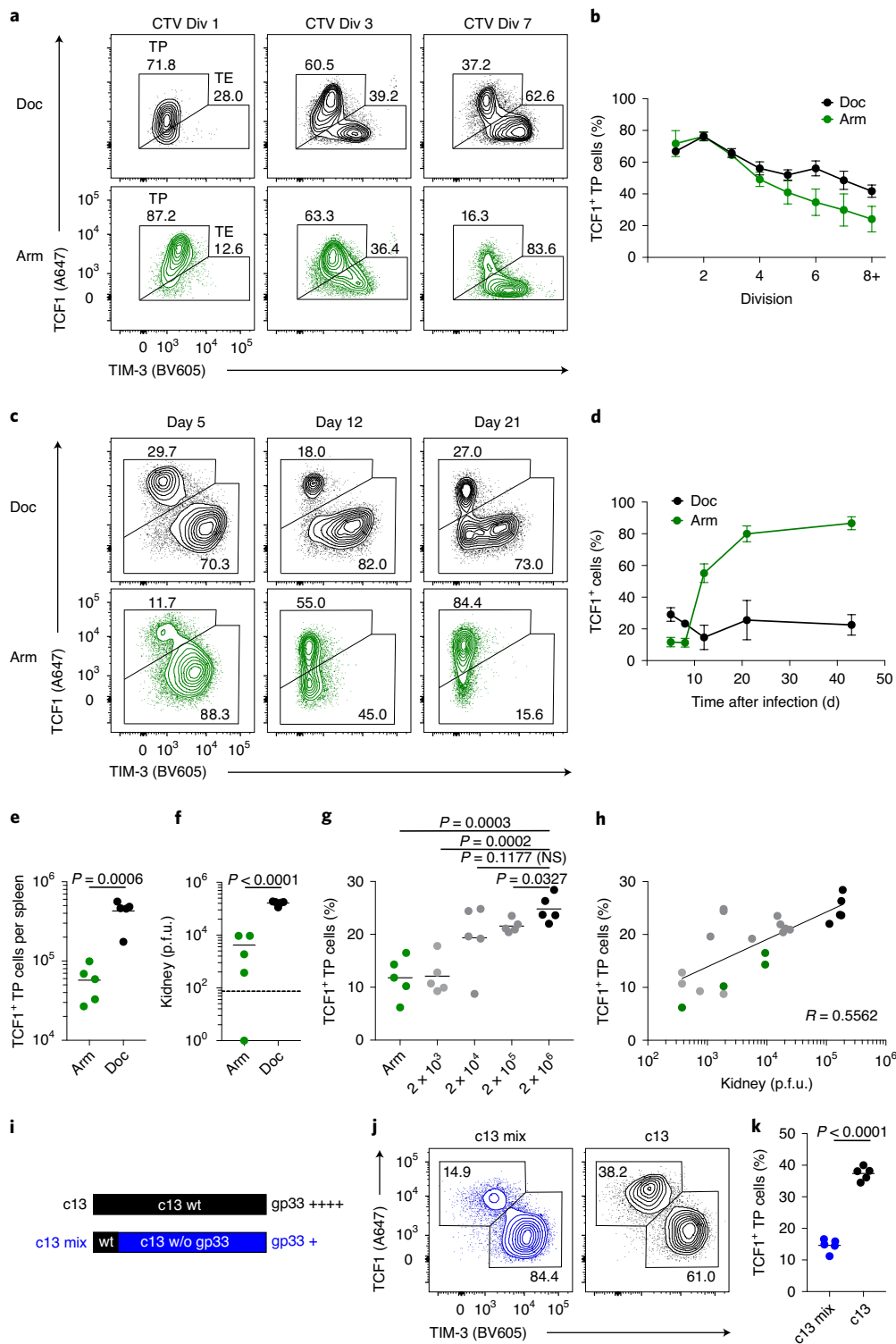


Fig. 1 | High amounts of antigen promote the differentiation of early TP cells. **a-d**, P14 T cells were labeled with CTV and transferred into congenically marked naive mice, infected with LCMV Docile (Doc, black) or Armstrong (Arm, green). Splenic P14 T cells were analyzed per cell division (Div), as described in Extended Data Fig. 1 (a,b) or at different times post-infection (c,d). **a,c**, TCF1 versus TIM-3 expression of P14 T cells. **b,d**, TP cell frequencies among P14 T cells. **e**, Numbers of TCF1⁺ TP cells on day 5 post-infection. **f**, Viral loads in kidneys on day 5 post-infection. The dotted line is the detection limit. **g**, TCF1⁺ P14 TP cell frequencies responding to titrated doses of Docile or 2×10^5 p.f.u. of Armstrong on day 5 post-infection. **h**, Correlation between TCF1⁺ TP cell frequencies and viral loads in the kidneys of mice infected with titrated doses of Docile (black/gray) or Armstrong (green) on day 5 post-infection. **i**, Schematic description of mixed infections in **j** and **k**. P14 T cells were transferred into congenically marked naive mice, infected with either wild-type LCMV clone-13 alone (c13, black) or mixed 1:10 with a mutant gp33-deficient clone-13 strain (c13 mix, blue). MFI, mean fluorescence intensity. **j**, TCF1 versus TIM-3 expression of P14 T cells on day 5 post-infection. **k**, TCF1⁺ P14 TP cell frequencies. Symbols represent the means of either three technical replicates (b) or four mice (d). Symbols in **e-k** represent individual mice; horizontal lines indicate the means. Data in **e-k** represent at least two experiments with five mice. Error bars indicate the s.e.m. Statistical analyses were performed using an unpaired, two-tailed Student's t-test. NS, not significant.

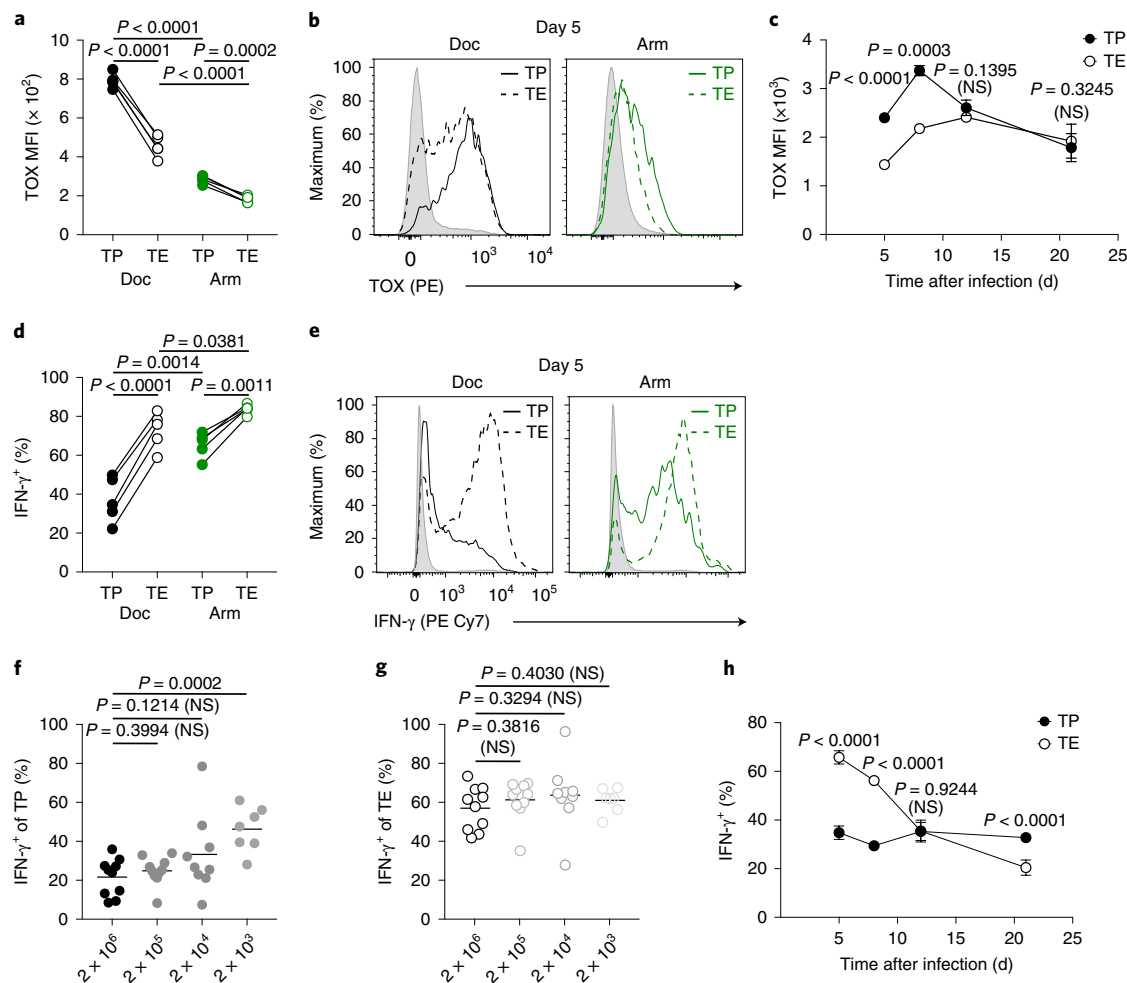


Fig. 2 | Early TP cells express high levels of TOX and are impaired in IFN- γ production. P14 T cells were transferred into congenically marked naive mice, which were infected with either LCMV Armstrong or titrated doses of Docile. **a,b**, TOX expression of TCF1 $^+$ TP (solid line) and TIM-3 $^+$ TE (dashed line) P14 T cells in mice infected with high-dose Docile (black) or Armstrong (green) on day 5 post-infection. Graphs show MFI of TP and TE P14 cells (**a**) and representative histograms (**b**); gray, host CD8 $^+$ T cells. **c**, TOX expression among splenic TP (solid dots) and TE (open dots) P14 T cells from high-dose Docile-infected mice. **d,e**, IFN- γ production from TP and TE cells after gp33-peptide re-stimulation, day 5 post-infection. TP and TE cell segregation based on Ly108 and TIM-3. Graphs show percent of IFN- γ + of TP and TE P14 cells (**d**) and representative histograms (**e**); gray, host CD8 $^+$ T cells. **f,g**, IFN- γ production from TP (**f**) and TE (**g**) cells responding to titrated doses of Docile after gp33-peptide re-stimulation on day 5 post-infection. **h**, IFN- γ production of TP and TE cells after gp33-peptide re-stimulation at indicated time points post-infection with high-dose Docile. Symbols in **a**, **d**, **f** and **g** represent individual mice; the lines connect P14 T cells within the same host. Symbols in **c** represent the mean of five mice and symbols in **h** at least nine mice pooled from two to three experiments. Data are combined or represent at least two independent experiments with at least four mice per group. Error bars indicate the s.e.m. Statistical analyses were performed using a paired Student's *t*-test when comparing TP and TE cells within the same mice or with an unpaired, two-tailed Student's *t*-test. NS, not significant.

Docile-infected mice with corresponding ID3 $^+$ and ID3 $^-$ memory populations in Armstrong-infected mice at day 21 post-infection (see Extended Data Fig. 5a–c). In total, we detected 1,764 DE genes, of which 281 were common to both comparisons, including *Pdcld1*, *Lag3* and *Tox*, constituting a ‘core exhaustion signature’ (see Extended Data Fig. 5a–c and Extended Data Table 5). Unsupervised clustering of the signature genes across all samples showed that early TP cells derived from Docile-infected mice clustered among other Docile-derived T cell populations (black dashed box, Fig. 4d,e). In contrast, early TE cells from the same Docile-infected mice clustered with the effector and memory populations derived from Armstrong-infected mice (green dashed box, Fig. 4d,e). Gene set enrichment analysis revealed that early TP cells derived from Docile-infected mice were highly enriched for genes upregulated in exhausted T cells, whereas TE cells from the same mice, as well as early TP cells from Armstrong-infected mice, were enriched for

genes upregulated in polyfunctional cells (Fig. 5f,g). Similar results were obtained when performing gene set enrichment analysis with a previously published exhaustion signature (see Extended Data Fig. 5d–f)^{9,11}. Thus, TP cells are first in acquiring the transcriptional features of exhausted T cells.

Epigenetic profile of early TP cells. T cell exhaustion is tightly linked to changes within the chromatin landscape^{25,31,32}. To test whether exhaustion-specific epigenetic marks accompanied the transcriptional profiles of early TP and TE cells, we isolated ID3 $^+$ and ID3 $^-$ P14 T cells early (day 5) and late (day 21) after Docile and Armstrong infections and performed an assay for transposase-accessible chromatin sequencing (ATAC-seq). MDS analysis showed that naive and memory T cells (day 21 Armstrong), regardless of their ID3 expression, clustered separately from T cells in ongoing infections (Fig. 5a). TE cells from Docile infection clustered closely together with T cell

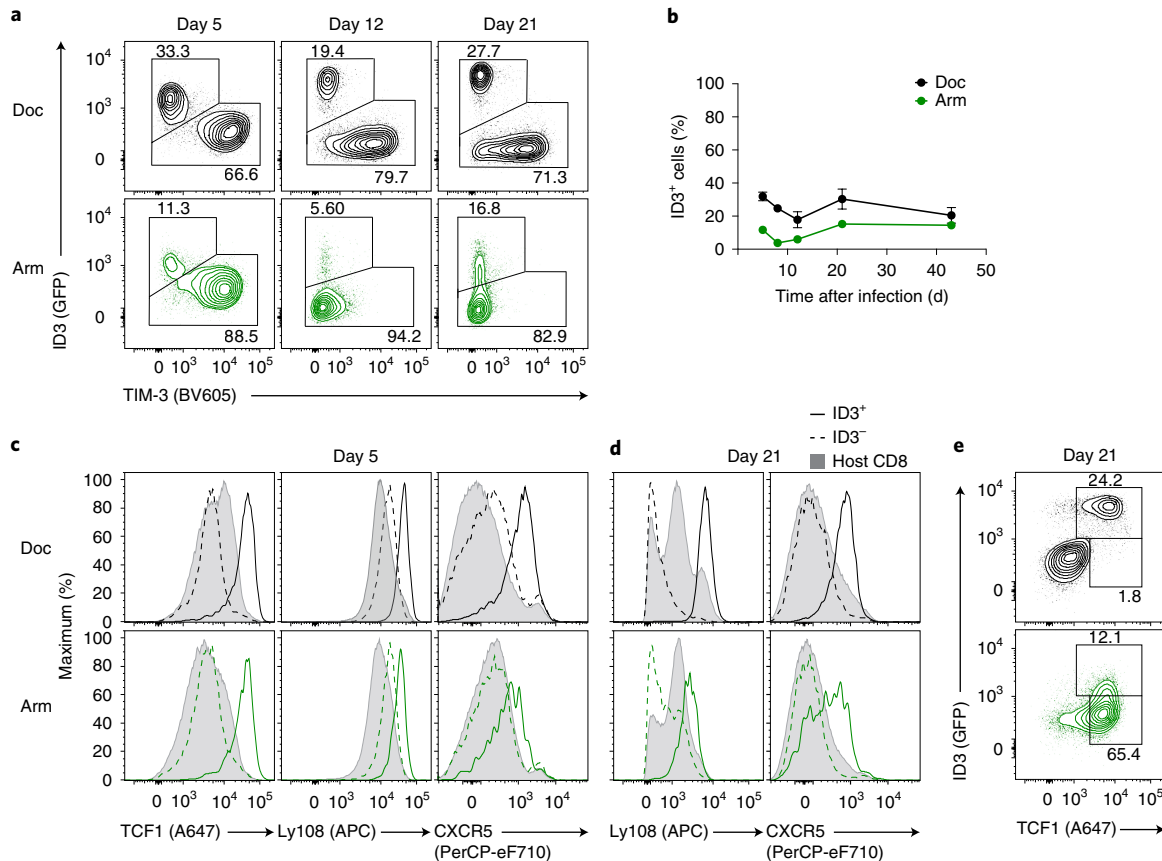


Fig. 3 | ID3 demarcates precursor T cells in acute and chronic infections. *Id3*^{GFP} P14 T cells were transferred into congenically marked naive recipient mice, which were infected with either LCMV Docile or Armstrong. **a**, ID3 versus TIM-3 expression of splenic P14 T cells on days 5, 12 and 21 post-infection with Docile (top, black) or Armstrong (bottom, green). GFP, green fluorescent protein. **b**, Frequencies of ID3⁺ cells among P14 T cells. **c**, Expression of TCF1, Ly108 and CXCR5 among ID3⁺ precursor (TP, solid lines) and ID3⁻ effector (TE, dashed lines) P14 T cells on day 5 post-infection with Docile (top, black), or Armstrong (bottom, green). **d**, Expression of Ly108 and CXCR5 among ID3⁺ TP (solid lines) and ID3⁻ TE (dashed lines) cells on day 21 post-infection with Docile (top, black) or Armstrong (bottom, green). **e**, ID3 versus TCF1 expression of splenic P14 T cells at day 21 post-infection with Docile (top, black) or Armstrong (bottom, green). Symbols in **b** are the mean of five mice. Data represent at least two independent experiments with five mice per group. Error bars indicate the s.e.m.

populations derived from early (day 5) Armstrong infections. In contrast, early and mature TP cells from Docile-infected mice clustered closely together and were well separated from other T cells in ongoing infections (Fig. 5a, dimension 2). We then identified chromatin regions that were differentially accessible and selected those corresponding to genes in our core exhaustion signature (see Extended Data Fig. 5c) to create an unsupervised clustered heatmap. Similar to our MDS analysis, early and mature TP cells from Docile-infected mice clustered together (Fig. 5b,c). They also clustered with mature TE cells from Docile-infected mice (Fig. 5b,c), indicating that the epigenetic profile of early TP cells from Docile-infected mice resembled that of fully exhausted T cells. In contrast, early TE cells from Docile-infected mice clustered closely with the samples derived from Armstrong-infected mice (Fig. 5b,c). In line with this notion, the *Tox* locus showed elevated accessibility specifically in early TP cells compared with early TE cells from Docile-infected mice (Fig. 5d), supporting the idea that exhaustion-specific chromatin changes occur first in TP cells. Notably, the *Pdcd1* locus (encoding PD-1) showed enhanced accessibility in all Docile-derived subsets, including day 5 TE cells (see Extended Data Fig. 6). Thus, TP cells in chronic infections are the first to acquire the epigenetic and transcriptional profiles of exhausted T cells.

BACH2 and BATF regulate early TP cell differentiation. Next, we analyzed DNA-binding motifs of transcription factors specifically

enriched in open chromatin regions of TP and TE cells. Regions more accessible in early Docile-derived TP cells compared with early TE cells showed strong enrichment of DNA-binding motifs of TCF1 and transcription factors of the JUN, AP-1 and NFAT families (Fig. 6a). This is consistent with the central roles of TCR-responsive transcription factors in T cell exhaustion^{15–17,33} and well aligned with the function of c-Jun in the long-term maintenance of chimeric antigen receptor T cells in cancer³⁴. Regions more accessible in TE cells were enriched for motifs of the T-box transcription factors T-BET and EOMES (Fig. 6a and Extended Data Tables 6 and 7). Of note, early TP cells, but not TE cells from Docile-infected mice, showed enrichment of DNA-binding motifs of BACH2 (Fig. 6a), a transcription factor that promotes memory T cell development in acute infections by limiting TCR-induced transcriptional changes³⁵, and the *Bach2* gene locus itself showed a strong increase in accessibility in TP cells (see Extended Data Fig. 7a). Correspondingly, *Bach2* was expressed at higher levels in early TP cells compared with TE cells from Docile-infected mice, a difference that became more pronounced in mature TP cells compared with TE cells (Fig. 6b,c).

To test the requirement of BACH2 for TP cell differentiation, we co-transferred P14 T cells lacking BACH2 (*Bach2*^{fl/fl}*Cd4*^{Cre}; *Bach2*^{-/-}) and control P14 T cells (*Cd4*^{Cre}) into congenically marked naive mice that were infected with LCMV Docile. Five days post-infection, BACH2-deficient T cells showed an impairment in generating TP cells whereas the expression of PD-1 and TOX was unaltered

(Fig. 6d–f). In contrast, overexpression of BACH2 strongly enforced TP cell generation, yet with reduced expression of PD-1 and TOX (Fig. 6g–i). Mechanistically, overexpression of BACH2 inhibits the function of IRF4 and transcription factors of the AP-1 family that promote expansion, effector differentiation and exhaustion^{35,36}. In line with this notion, deletion of the AP-1 transcription factor BATF, recently shown to be critical for anti-tumor T cell responses³⁷, resulted in a strong bias toward the generation of TP cells and impaired expression of PD-1 and TOX (Fig. 6j–l), similar to the overexpression of BACH2. As regulated expression of BATF is required for efficient population expansion^{16,38,39}, its deletion or suppression through the overexpression of its competing factor BACH2 resulted in reduced numbers of both TP and TE cells (Fig. 6e,h,k). However, consistent with our conclusion that BACH2 and BATF regulated TP cell generation in an opposing manner, numbers of TP cells were more affected by the loss of BACH2, whereas they were relatively favored in conditions of reduced BATF activity (BACH2 overexpression) or BATF deficiency. Of note, the substantial loss of *Bach2*^{-/-} P14 TP and TE cells was mainly due to increased initial cell death after transfer (data not shown). This notion was supported by the observation that *Bach2*^{fl/fl}*Cd4*^{Cre} mice without the P14 transgene were able to mount a gp33⁺ CD8 T cell response of similar magnitude to control mice, whereas TP cell generation remained impaired (see Extended Data Fig. 7b,c). T cells lacking BACH2 or BATF also showed skewed generation of TP and TE cells in response to LCMV Armstrong infection, indicating that the role of this transcriptional module is conserved across different infections (see Extended Data Fig. 7d–g). However, the effects were larger in conditions of chronic infection, in line with the prominent role of BATF in T cell exhaustion¹⁶. Overall, we identified BACH2 and BATF as critical factors that regulate the generation of TP cells in a competing manner.

Exhaustion is imprinted in early TP cells. Antigen-specific T cells obtained from established chronic infections stably maintain their exhausted phenotype even after antigen withdrawal and population re-expansion in an acute infection⁴⁰, an observation consistent with epigenetic imprinting of T cell exhaustion^{31,32,41}. To determine whether exhaustion features of early TP cells were stably imprinted and propagated to their progeny, we isolated TP and TE cells from day 5 Docile- and Armstrong-infected mice and transferred them into naive hosts, which were challenged with an acute Armstrong infection (Fig. 7a). Although all populations retained substantial proliferative potential (Fig. 7b), expanding TP cells from Docile-infected mice sustained higher expression of PD-1 and TOX compared with expanding TE cells from the same mice, or compared with expanding TP and TE cells from Armstrong-infected mice (Fig. 7c,d), indicating that early features of exhaustion were imprinted in TP cells. Consistent with this conclusion, even memory T cells derived from early TP cells from Docile-infected mice sustained elevated TOX levels long after antigen clearance (Fig. 7e,f). In line with published studies^{31,32,41} and our molecular data, imprinting of exhaustion features increased over time, as seen by the reduced recall potential and increased expression of TOX and

PD-1 in re-expanded TP cells isolated at day 26 compared with day 5 after Docile infection (see Extended Data Fig. 8).

Finally, to test the proliferative potential of early LCMV-specific T cell populations in conditions of chronic infection, we isolated early TP and TE cells from day 5 Docile- and Armstrong-infected mice, transferred them into time-matched Docile-infected mice and analyzed 7 or 17 days post-transfer (Fig. 7g). Strikingly, early TE cells derived from either Armstrong or Docile infection were unable to mount a functional T cell response under conditions of persistent antigen stimulation, whereas early TP cells derived from either infection were able to expand robustly (Fig. 7h). However, consistent with early exhaustion, Docile-derived TP cells, compared with Armstrong-derived TP cells, showed an impaired expansion as well as reduced ability to maintain TCF1 expression and generate CX3CR1⁺ cells (Fig. 7h,i), recently identified as direct progeny of TCF1⁺ cells in chronic infection^{23,24}. In summary, our data show that TP cells during chronic infection are the first to acquire stably imprinted features of exhaustion.

Discussion

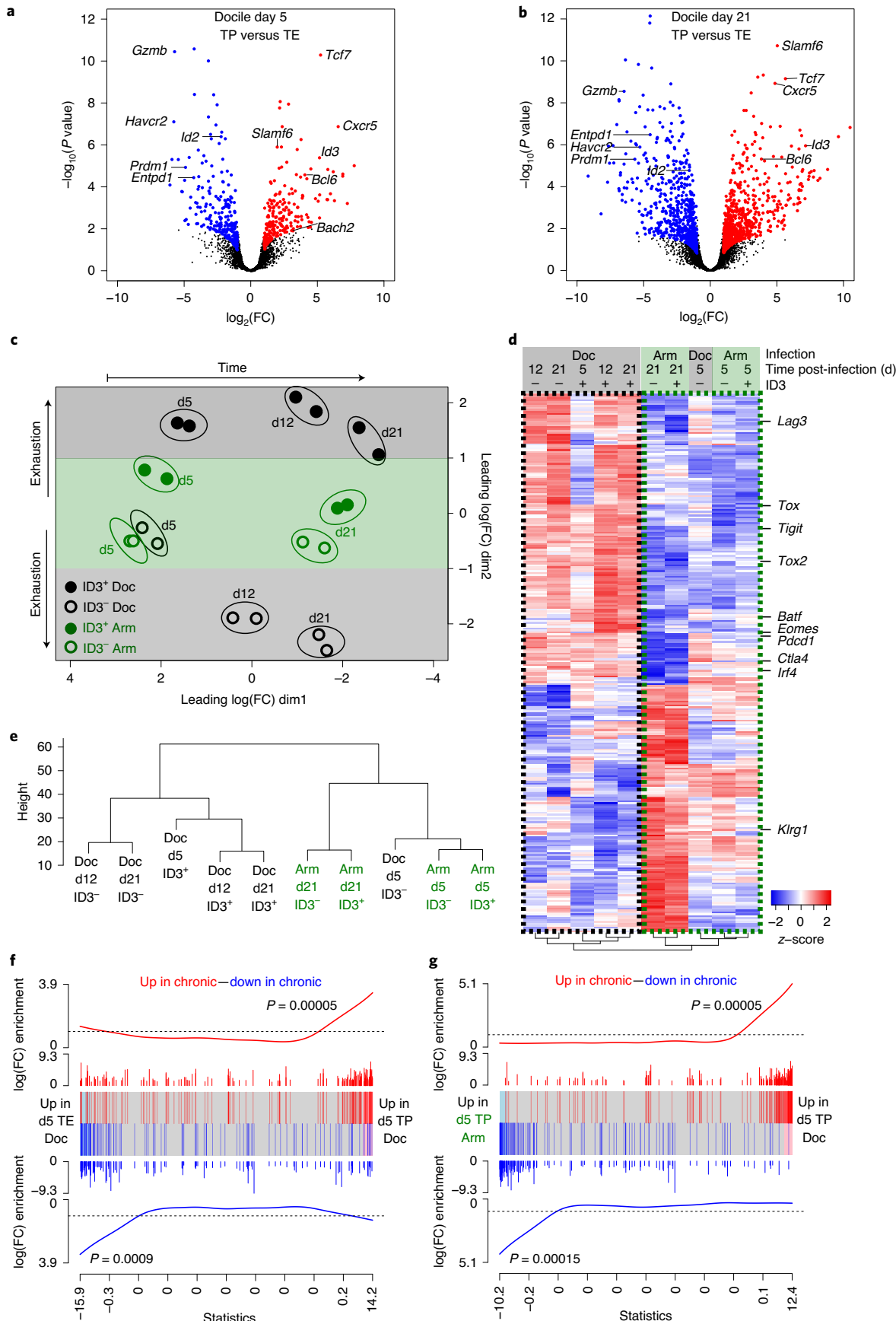
T cells responding to chronic antigen stimulation are sustained by a subset of precursor cells that self-renew while also generating exhausted effector cells^{7,8,19,20}. However, the mechanisms that lead to the establishment of a precursor–progeny hierarchy during chronic infection remain incompletely understood. In the present study, we show that high antigenic load facilitated the differentiation of virus-specific TCF1⁺ID3⁺ TP cells early during infection. Although the early dichotomy of antigen-specific T cell differentiation into precursor and effector-fated cells was similar in chronic and acute infections, increased amounts of antigen promoted differentiation of TP cells, which showed early characteristics of exhaustion. In line with this observation, early TP cells, in response to both chronic and acute infections, had a lower ability to produce IFN-γ and expressed elevated levels of TOX compared with early TE cells. These observations suggest that high amounts of antigen initiate molecular pathways that protect TP cells from undergoing full differentiation, and thus preserve their proliferative and developmental potential.

Our data show that initial levels of antigen not only control the precursor versus effector dichotomy, but also critically impact the early acquisition of features of T cell exhaustion. Indeed, early TP cells (day 5) responding to LCMV Docile infection acquired transcriptional and epigenetic profiles similar to those of mature (day 21) TPEX cells found in established chronic infections. This included elevated expression of PD-1 and TOX in TP cells, which was propagated to their progeny even in conditions of acute infection. Indeed, the chromatin profile of TP cells derived early from Docile-infected mice was already similar to that of mature TPEX cells isolated late from Docile-infected mice, highlighting that the exhaustion program is initiated early during T cell activation, and at least to some degree inheritably imprinted. However, our data also show that epigenetic imprinting and acquisition of the transcriptional profile of exhaustion are progressive. This is well in line with a series of studies showing that continuous TCR stimulation drives

Fig. 4 | Early TP cells in chronic infection acquire an exhausted phenotype. *Id3*^{GFP} P14 T cells were transferred into naive recipient mice, which were infected with either LCMV Armstrong or Docile. ID3⁺TIM-3⁻ and ID3⁻TIM-3⁺ P14 T cells were purified for RNA-seq analysis from mice at days 5, 12 and 21 post-infection with Docile or Armstrong as indicated. **a,b**, Volcano plots showing DE genes between ID3⁺TIM-3⁻ and ID3⁻TIM-3⁺ P14 T cells obtained from Docile-infected mice on day (d) 5 (**a**) or day 21 (**b**) post-infection. **c**, MDS plot with boxes highlighting exhausted (black) and polyfunctional (green) phenotypes. dim, dimension. **d**, Heatmap established by unsupervised clustering of all samples based on the ‘core exhaustion signature’ from Extended Data Fig. 5c. Green and black boxes at the top highlight the origin of the cell subsets (black, Docile; green, Armstrong). Dotted squares highlight the main two clusters: green square, polyfunctional phenotype; black square, exhausted phenotype. **e**, Hierarchical tree of unsupervised clustered heatmap. **f,g**, Gene set enrichment analyses based on ROAST tests. Barcode plots show enrichment of genes upregulated (red) and genes downregulated (blue) in the ‘core exhaustion signature’ Docile ID3⁺TIM-3⁻ TP versus ID3⁻TIM-3⁺ TE cells (**f**), or Docile TP versus Armstrong TP cells (**g**) on day 5 post-infection. RNA-seq analysis was performed with two experimental replicates at each time point. The unsupervised heatmap is based on merged replicates.

stable imprinting of T cell exhaustion in a time-dependent manner^{31,32,41}. TCR-inducible transcription factors, such as NFATC1, IRF4, BATF and TOX, play central roles in the differentiation of

exhausted T cells^{11–17}. In the present study, we extend these observations by demonstrating that BACH2 and BATF act in an opposing fashion to regulate generation and phenotype of early TP cells,



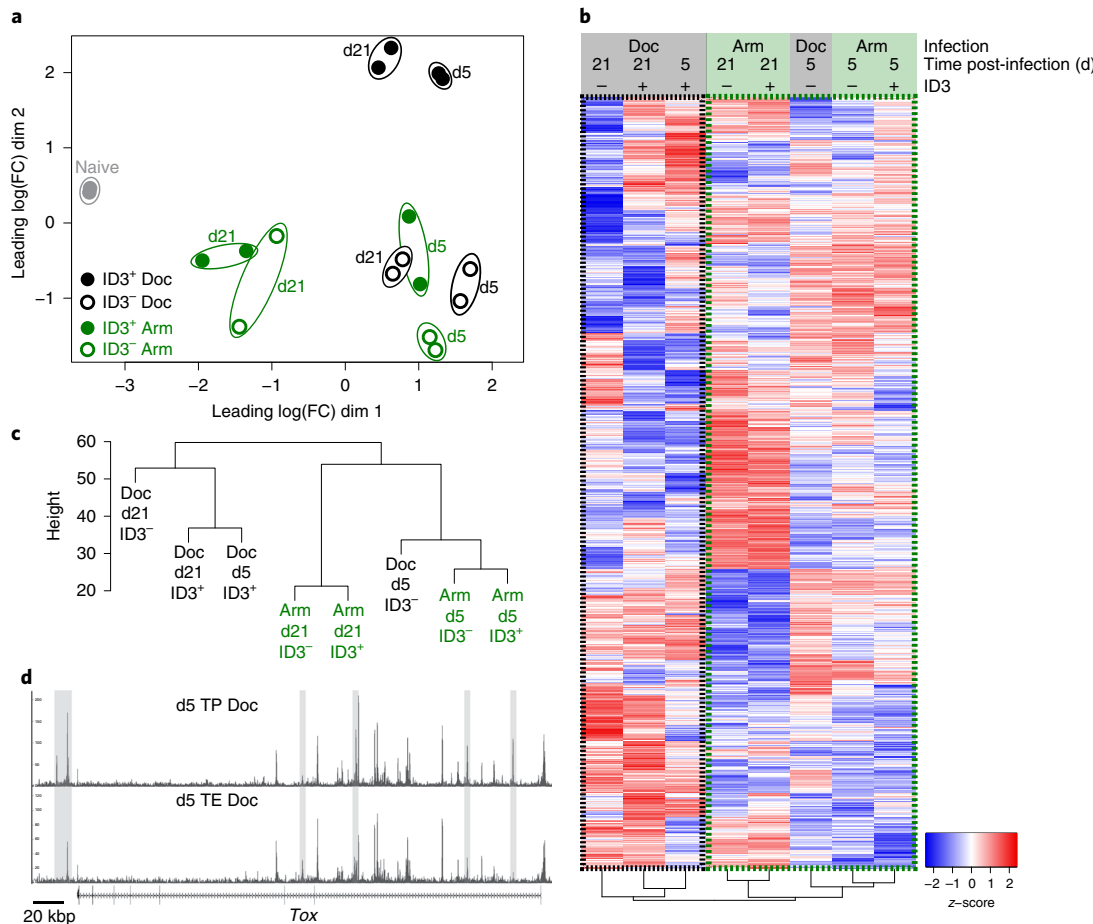


Fig. 5 | Early TP cells in chronic infection acquire the epigenetic profile of exhausted T cells. Congenically marked *Id3*^{GFP} P14 T cells were transferred into naive recipient mice, which were infected with either LCMV Armstrong or Docile. On days (d) 5 and 21 post-infection, ID3⁺TIM-3⁻ and ID3-TIM-3⁺P14 T cells were purified and chromatin accessibility determined by ATAC-seq. **a**, MDS plot analysis of all samples. dim, dimension. **b**, Unsupervised clustering of all samples based on differentially accessible peaks assigned to ‘core exhaustion signature’ genes (see Extended Data Fig. 5c). Green and black boxes at the top highlight the origin of the cells (green, Armstrong; black, Docile). Dotted boxes highlight the two main clusters. **c**, Hierarchical tree of unsupervised clustered heatmap. **d**, Chromatin accessibility of *Tox* locus of Docile-derived ID3⁺TIM-3⁻ TP and ID3-TIM-3⁺ TE cells at day 5 post-infection. Gray boxes highlight regions that are differentially accessible between the two samples. ATAC-seq analysis was performed with two experimental replicates at each time point. Open chromatin tracks are based on merged replicates.

and thus might critically impact the long-term T cell response to chronic infections.

Our study shows that TP cells are programmed early with an elevated developmental potential for long-term maintenance, and provides further evidence for their essential role in sustaining the T cell response during chronic infection. Importantly, this holds true for early TP cells responding to acute infection as well as for TPEX cells responding to an overwhelming infection that might persist for extended periods. Thus, despite displaying reduced effector function already early during the infection, TP cells maintain a high proliferative and developmental potential. In contrast, early TE cells, despite exhibiting a polyfunctional profile, showed reduced proliferative potential and were unable to sustain a T cell response during chronic infection, supporting previous work showing that proliferative potential and functional exhaustion are uncoupled⁹.

Notably, the picture that emerges from our data is in stark contrast to the prevailing model of T cell differentiation in response to chronic infection, according to which effector cells progressively undergo transcriptional and epigenetic alterations that lead to impaired T cell function⁴². Our results suggest a model in which high antigen load facilitates the generation of TP cells, which acquire features of exhaustion early and, over time, generate exhausted TE

cells. Interestingly, our data show that early TE cells in chronic infection exhibit a polyfunctional profile similar to cells in acute infection. Only subsequently is this ‘first generation’ of fully functional TE cells replenished by a ‘second generation’ of functionally impaired TE cells. In contrast to the first generation, which derive from naive T cells, these second-generation effector cells derive from TP cells and display impaired effector function. This model is supported by recent observations that described a subset of KLRG1-expressing TE cells early (day 8) in chronic LCMV infection, which retained a higher ability to produce IFN- γ while lacking proliferative potential⁴³. They thus constitute a transient population that is largely absent by day 12 post-infection. Based on our data, we propose that the KLRG1⁺ T cell subset represents the first generation of TE cells similar to the ones we describe here for the early stage of infection. This subsequent replenishment of polyfunctional T cells with exhausted T cells creates a balance between viral or tumor control and immune-mediated pathology. Importantly, the mechanisms regulating and establishing this functional adaptation act early in response to overwhelming viral infections. This notion is of particular interest when considering T cell responses to overwhelming viral infections such as with SARS-CoV-2, which has been shown to induce an at least partially exhausted T cell response⁴⁴. Thus, our data highlight the potential

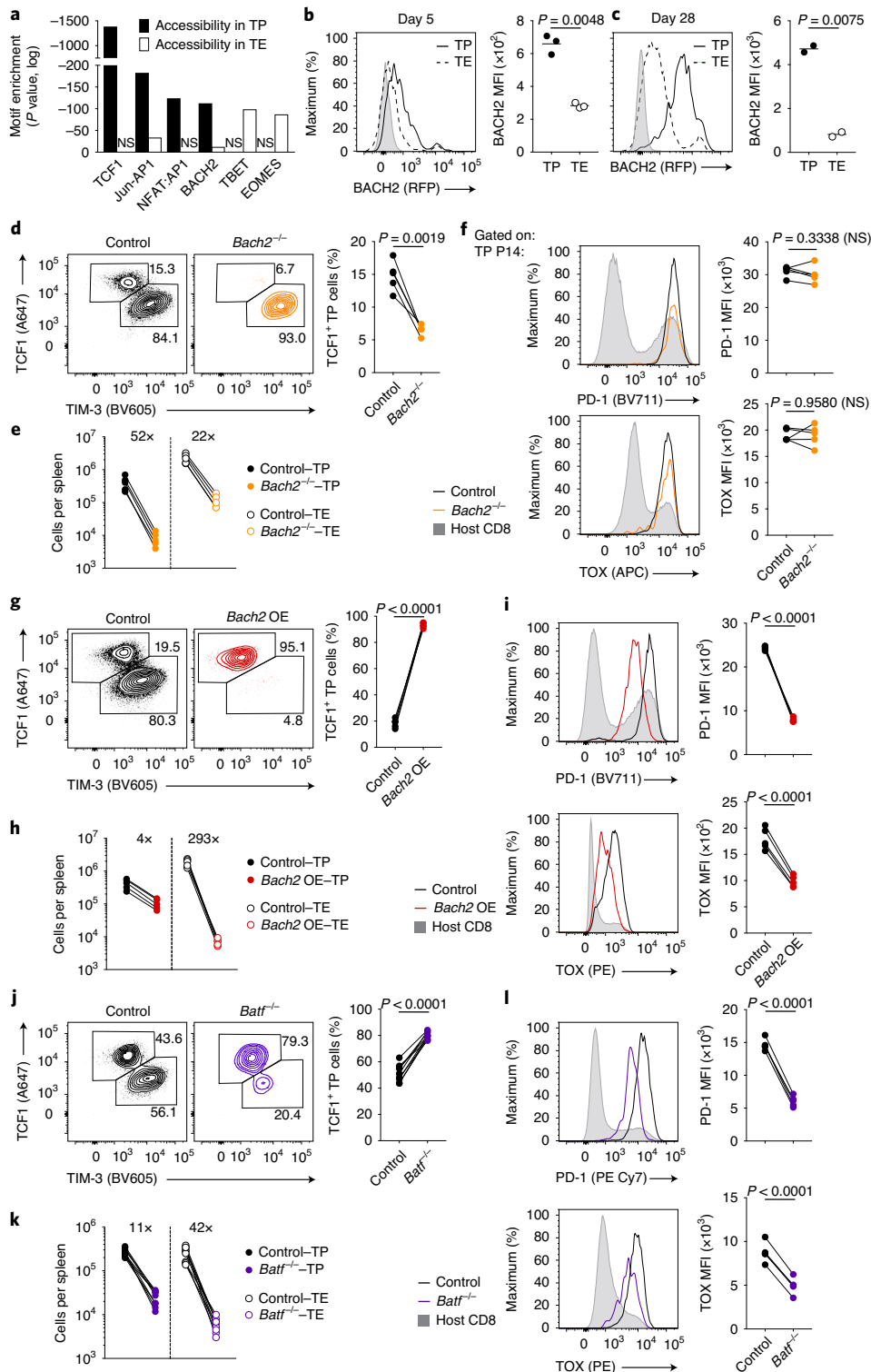


Fig. 6 | Early TP cell differentiation in chronic infection is regulated by BACH2 and BATF. **a**, Motif enrichment of transcription factors within chromatin regions more accessible in day 5 TP compared with TE cells (black bars) or more accessible in TE compared with TP cells (open bars), as identified by ATAC-seq (as in Fig. 5). **b,c**, *Bach2*^{fl/fl} mice were infected with LCMV Docile. BACH2 expression among gp33-tetramer⁺ TP (Ly108⁺TIM-3⁺) and TE (Ly108⁻TIM-3⁺) cells on days 5 (**b**) and 28 post-infection (**c**). RFP, red fluorescent protein. **d–l**, Congenically marked BACH2-deficient (*Bach2*^{fl/fl}*Cd4*^{Cre}, labeled as *Bach2*^{-/-}) and control (*Cd4*^{Cre}, labeled as control) P14 T cells. P14 T cells retrovirally transduced to overexpress BACH2 (*Bach2* OE) (**d–f**) or with control vector (**g–i**) or *Batf*^{fl/fl} and *Batf*^{fl/fl} control P14 T cells (**j–l**) were co-transferred into naive mice, which were infected with Docile and analyzed 5 d later. **d,g,j**, TCF1 versus TIM-3 and quantification of donor-derived TCF1⁺ TP cell frequencies in the spleen. **e,h,k**, Numbers of splenic TCF1⁺ TP and TIM-3⁺ TE cells on day 5 post-infection. Numbers above indicate the fold increase in controls versus *Bach2*^{-/-} (**e**), *Bach2* OE (**h**) or *Batf*^{fl/fl} (**k**). **f,i,l**, PD-1 and TOX expression among *Bach2*^{-/-} (**f**), *Bach2* OE (**i**) or *Batf*^{fl/fl} (**l**) TP cells compared with controls. Symbols in **b–l** represent individual mice; the lines connect P14 T cells within the same host. Data are combined (**j, k**) or represent at least two independent experiments with at least three mice per group. Error bars indicate the s.e.m. Statistical analyses were performed using a paired, two-tailed Student's *t*-test. NS, not significant.

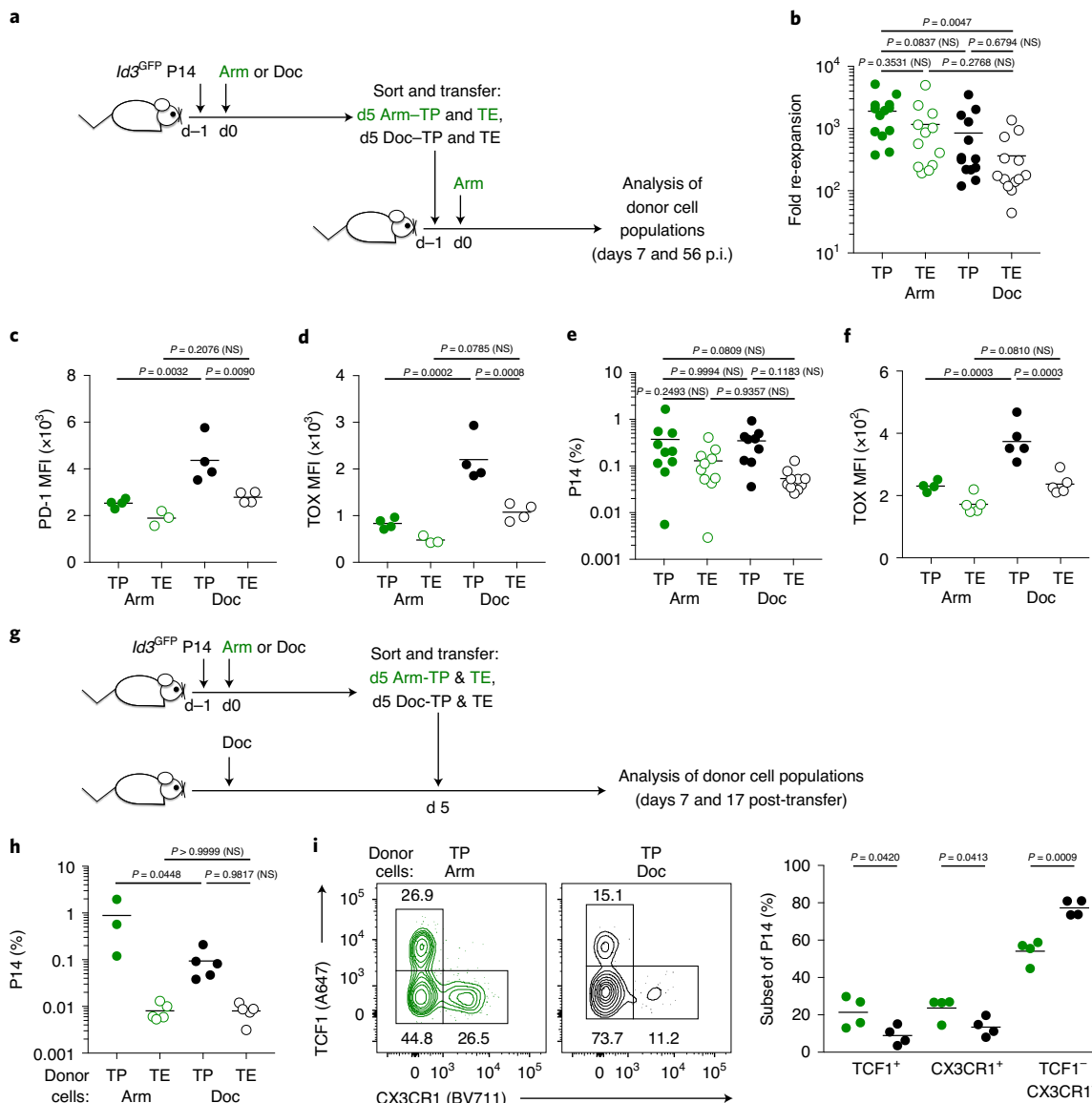


Fig. 7 | Early exhausted TP cells retain proliferative potential but are restricted to the generation of exhausted T cells. **a**, Experimental scheme for **b–f**. *Id3^{GFP}* P14 T cells were transferred into naive recipient mice that were infected with either LCMV Armstrong or Docile; 5 days post-infection, ID3⁺TIM-3⁻ TP and ID3-TIM-3⁺ TE P14 T cells were sorted and transferred into naive mice, which were infected with acute LCMV Armstrong. Donor P14 T cells were analyzed on days 7 or 56 post-transfer. **b–f**, Fold expansion. **c,d**, PD-1 (**c**) and TOX (**d**) expression of donor P14 T cells 7 days post-transfer. **e,f**, Frequencies (**e**) and TOX expression (**f**) of donor-derived P14 T cells 56 days post-transfer. **g**, Experimental scheme for **h** and **i**. *Id3^{GFP}* P14 T cells were transferred into naive mice that were infected with either Armstrong or Docile. Then 5 days post-infection, TP and TE cells were sorted as in **a** and transferred into time-matched, Docile-infected mice and analyzed on days 7 or 17 post-transfer. **h**, P14 T cell frequencies in the spleen on day 7 post-transfer. **i**, TCF1 and CX3CR1 expression of TP cell-derived progeny (left) and frequencies of donor-derived TCF1⁺, CX3CR1⁺ or TCF1⁻CX3CR1⁻ cells in the spleen on day 17 post-transfer (right). Symbols in **b–f**, **h** and **i** represent individual mice; horizontal lines indicate means. Data are combined or represent at least two experiments (**b–f**, **h**) or one experiment per time point (**h**, **i**) with at least three mice per group. Statistical analyses were performed using a one-way ANOVA multiple-comparison test (**b–f**, **h**) or an unpaired, two-tailed Student's t-test (**i**). NS, not significant.

to target molecules associated with T cell exhaustion early during a severe infection to improve antiviral immunity.

Overall, our data suggest that T cell exhaustion is an active process that, in situations of high and sustained antigenic load, protects TPEX cells from undergoing full differentiation. Indeed, enhanced expression of exhaustion-associated molecules such as PD-1 and TOX, early after activation in situations of high antigen exposure, places a brake on TPEX cells, allowing their preservation during ongoing infections while reducing the risk of immune-mediated collateral damage. Such a mechanism is an evolutionarily use-

ful adaptation that allows for the maintenance of T cell responses during protracted infections or tumor growth while protecting the organism from immune pathology.

Online content

Any methods, additional references, Nature Research reporting summaries, extended data, supplementary information, acknowledgements, peer review information; details of author contributions and competing interests; and statements of data and code availability are available at <https://doi.org/10.1038/s41590-020-0760-z>.

Received: 13 March 2020; Accepted: 10 July 2020;
Published online: 24 August 2020

References

1. McLane, L. M., Abdel-Hakeem, M. S. & Wherry, E. J. CD8 T cell exhaustion during chronic viral infection and cancer. *Annu. Rev. Immunol.* **37**, 457–495 (2019).
2. Hashimoto, M. et al. CD8 T cell exhaustion in chronic infection and cancer: opportunities for interventions. *Annu. Rev. Med.* **69**, 301–318 (2018).
3. Kuchroo, V. K., Anderson, A. C. & Petrovas, C. Coinhibitory receptors and CD8 T cell exhaustion in chronic infections. *Curr. Opin. HIV AIDS* **9**, 439–445 (2014).
4. Klebanoff, C. A., Gattinoni, L. & Restifo, N. P. CD8⁺ T-cell memory in tumor immunology and immunotherapy. *Immunol. Rev.* **211**, 214–224 (2006).
5. Baitsch, L. et al. Exhaustion of tumor-specific CD8⁺ T cells in metastases from melanoma patients. *J. Clin. Invest.* **121**, 2350–2360 (2011).
6. Ahmadzadeh, M. et al. Tumor antigen-specific CD8 T cells infiltrating the tumor express high levels of PD-1 and are functionally impaired. *Blood* **114**, 1537–1544 (2009).
7. Lugli, E., Galletti, G., Boi, S. K. & Youngblood, B. A. Stem, effector, and hybrid states of memory CD8⁺ T cells. *Trends Immunol.* **41**, 17–28 (2020).
8. Kallies, A., Zehn, D. & Utzschneider, D. T. Precursor exhausted T cells: key to successful immunotherapy? *Nat. Rev. Immunol.* **20**, 128–136 (2020).
9. Utzschneider, D. T. et al. High antigen levels induce an exhausted phenotype in a chronic infection without impairing T cell expansion and survival. *J. Exp. Med.* **213**, 1819–1834 (2016).
10. Angelosanto, J. M., Blackburn, S. D., Crawford, A. & Wherry, E. J. Progressive loss of memory T cell potential and commitment to exhaustion during chronic viral infection. *J. Virol.* **86**, 8161–8170 (2012).
11. Alfei, F. et al. TOX reinforces the phenotype and longevity of exhausted T cells in chronic viral infection. *Nature* **571**, 265–269 (2019).
12. Khan, O. et al. TOX transcriptionally and epigenetically programs CD8⁺ T cell exhaustion. *Nature* **571**, 211–218 (2019).
13. Yao, C. et al. Single-cell RNA-seq reveals TOX as a key regulator of CD8⁺ T cell persistence in chronic infection. *Nat. Immunol.* **20**, 890–901 (2019).
14. Scott, A. C. et al. TOX is a critical regulator of tumour-specific T cell differentiation. *Nature* **571**, 270–274 (2019).
15. Seo, H. et al. TOX and TOX2 transcription factors cooperate with NR4A transcription factors to impose CD8⁺ T cell exhaustion. *Proc. Natl Acad. Sci. USA* **116**, 12410–12415 (2019).
16. Man, K. et al. Transcription factor IRF4 promotes CD8⁺ T cell exhaustion and limits the development of memory-like T cells during chronic infection. *Immunity* **47**, 1129–1141.e5 (2017).
17. Martinez, G. J. et al. The transcription factor NFAT promotes exhaustion of activated CD8⁺ T cells. *Immunity* **42**, 265–278 (2015).
18. Wu, T. et al. The TCF1-Bcl6 axis counteracts type I interferon to repress exhaustion and maintain T cell stemness. *Sci. Immunol.* **1**, eaai8593 (2016).
19. Utzschneider, D. T. et al. T cell factor 1-expressing memory-like CD8⁺ T cells sustain the immune response to chronic viral infections. *Immunity* **45**, 415–427 (2016).
20. Im, S. J. et al. Defining CD8⁺ T cells that provide the proliferative burst after PD-1 therapy. *Nature* **537**, 417–421 (2016).
21. He, R. et al. Follicular CXCR5-expressing CD8⁺ T cells curtail chronic viral infection. *Nature* **537**, 412–428 (2016).
22. Leong, Y. A. et al. CXCR5⁺ follicular cytotoxic T cells control viral infection in B cell follicles. *Nat. Immunol.* **17**, 1187–1196 (2016).
23. Hudson, W. H. et al. Proliferating transitory T cells with an effector-like transcriptional signature emerge from PD-1⁺ stem-like CD8⁺ T cells during chronic infection. *Immunity* **51**, 1043–1058.e4 (2019).
24. Zander, R. et al. CD4⁺ T cell help is required for the formation of a cytolytic CD8⁺ T cell subset that protects against chronic infection and cancer. *Immunity* **51**, 1028–1042.e4 (2019).
25. Miller, B. C. et al. Subsets of exhausted CD8⁺ T cells differentially mediate tumor control and respond to checkpoint blockade. *Nat. Immunol.* **20**, 326–336 (2019).
26. Sade-Feldman, M. et al. Defining T cell states associated with response to checkpoint immunotherapy in melanoma. *Cell* **175**, 998–1013.e20 (2018).
27. Brummelman, J. et al. High-dimensional single cell analysis identifies stem-like cytotoxic CD8⁺ T cells infiltrating human tumors. *J. Exp. Med.* **215**, 2520–2535 (2018).
28. Siddiqui, I. et al. Intratumoral Tcf1⁺PD-1⁺CD8⁺T cells with stem-like properties promote tumor control in response to vaccination and checkpoint blockade immunotherapy. *Immunity* **50**, 195–211.e10 (2019).
29. Menner, A. J. et al. Id3 controls cell death of 2B4⁺ virus-specific CD8⁺ T cells in chronic viral infection. *J. Immunol.* **195**, 2103–2114 (2015).
30. Kaech, S. M. & Wherry, E. J. Heterogeneity and cell-fate decisions in effector and memory CD8⁺ T cell differentiation during viral infection. *Immunity* **27**, 393–405 (2007).
31. Pauken, K. E. et al. Epigenetic stability of exhausted T cells limits durability of reinvigoration by PD-1 blockade. *Science* **354**, 1160–1165 (2016).
32. Sen, D. R. et al. The epigenetic landscape of T cell exhaustion. *Science* **354**, 1165–1169 (2016).
33. Oestreich, K. J., Yoon, H., Ahmed, R. & Boss, J. M. NFATc1 regulates PD-1 expression upon T cell activation. *J. Immunol.* **181**, 4832–4839 (2008).
34. Lynn, R. C. et al. c-Jun overexpression in CAR T cells induces exhaustion resistance. *Nature* **576**, 293–300 (2019).
35. Roychoudhuri, R. et al. BACH2 regulates CD8⁺ T cell differentiation by controlling access of AP-1 factors to enhancers. *Nat. Immunol.* **17**, 851–860 (2016).
36. Sidwell, T. et al. Attenuation of TCR-induced transcription by Bach2 controls regulatory T cell differentiation and homeostasis. *Nat. Commun.* **11**, 252 (2020).
37. Wei, J. et al. Targeting REGNASE-1 programs long-lived effector T cells for cancer therapy. *Nature* **576**, 471–476 (2019).
38. Xin, G. et al. A critical role of IL-21-induced BATF in sustaining CD8-T-cell-mediated chronic viral control. *Cell Rep.* **13**, 1118–1124 (2015).
39. Grusdat, M. et al. IRF4 and BATF are critical for CD8⁺ T-cell function following infection with LCMV. *Cell Death Differ.* **21**, 1050–1060 (2014).
40. Utzschneider, D. T. et al. T cells maintain an exhausted phenotype after antigen withdrawal and population reexpansion. *Nat. Immunol.* **14**, 603–610 (2013).
41. Ghoneim, H. E. et al. De novo epigenetic programs inhibit PD-1 blockade-mediated T cell rejuvenation. *Cell* **170**, 142–157.e19 (2017).
42. Blank, C. U. et al. Defining 'T cell exhaustion'. *Nat. Rev. Immunol.* **19**, 665–674 (2019).
43. Chen, Z. et al. TCF-1-centered transcriptional network drives an effector versus exhausted CD8 T cell-fate decision. *Immunity* **51**, 840–855.e5 (2019).
44. Diao, B. et al. Reduction and functional exhaustion of T cells in patients with coronavirus disease 2019 (COVID-19). *Front. Immunol.* **11**, 827 (2020).

Publisher's note Springer Nature remains neutral with regard to jurisdictional claims in published maps and institutional affiliations.

© The Author(s), under exclusive licence to Springer Nature America, Inc. 2020

Methods

Mice. Wild-type C57BL/6JArc mice on a Ly5.1 or Ly5.2 background were obtained from the Australian Resources Center. *Id3*^{GFP} (ref. ⁴⁵), *Bach2*^{fl/fl} (ref. ⁴⁶), *Cd4*^{Cre} (ref. ⁴⁷), *Bach2*^{RFP} (ref. ⁴⁸) and *Batf*^{-/-} (ref. ¹⁴) mice have been previously described, and crossed to include the P14 TCR transgene (JAX: Tg(TcrLCMV)327Sdz) for some experiments. All mice were maintained and used in accordance with the guidelines of the University of Melbourne Animal Ethics Committee.

LCMV infections. LCMV Armstrong, clone-13 and Docile were propagated and quantified as previously described⁴⁰. Frozen stocks were diluted in phosphate-buffered saline (PBS); 2×10^5 plaque-forming units (p.f.u.) of LCMV Arm were injected intraperitoneally, and 2×10^6 p.f.u. of LCMV clone-13 or Docile or titrated doses as indicated were injected intravenously. The previously described mixed-mutant infection^{9,11} was performed by co-injecting 1.8×10^6 p.f.u. of a gp33-deficient LCMV clone-13 mutant (A3 strain, encoding an H-2D^b-binding-deficient, gp33-altered peptide ligand⁴⁹) along with 2×10^5 p.f.u. of wild-type LCMV clone-13. Kidneys from LCMV-infected mice were 'shock frozen' before homogenization. Diluted suspensions were used for infection of Vero cells, and viral titers were determined by an LCMV focus-forming assay⁵⁰.

Purification of mouse T cells and adoptive T cell transfer. Single-cell splenocyte suspensions were obtained by mashing total spleens through a 70-μm nylon cell strainer (BD), and red blood cells were lysed with a hypotonic ammonium chloride-potassium bicarbonate buffer. Transgenic naive P14 T cells were isolated using the mouse CD4⁺ T cell enrichment kit (Miltenyi Biotech), and 3,000–10,000 P14 T cells were intravenously injected into naive congenically marked recipients. For cell division tracking, purified P14 were labeled with 5 μM CellTrace Violet (CTV, Invitrogen) for 10 min at 37 °C before cell transfer.

For re-isolation of *Id3*^{GFP} P14 T cells in transfer experiments, RNA-seq or ATAC-seq, P14 T cells were pre-enriched by staining total splenocytes in Dulbecco's modified Eagle's medium supplemented with 10% fetal bovine serum with biotin-labeled anti-Ly5.1 or anti-Ly5.2 antibodies, followed by anti-biotin beads and positive selection on magnetic columns (Miltenyi Biotech). Pre-enriched samples were then stained with CD8a (1:200, Thermo Fisher Scientific, clone 53-6.7), Ly5.1 (1:200, BD, clone A20), Ly5.2 (1:800, Walter and Eliza Research Institute (WEHI), clone 104) and TIM-3 (1:200, BioLegend, clone RMT3-23). ID3(GFP)⁺TIM-3⁺T_p and ID3(GFP)⁺TIM-3⁺TE cells were isolated by FACS. TP or TE P14 T cells, $2 \times 9 \times 10^4$, were transferred per experiment. The fold expansion of P14 T cells in secondary hosts was determined relative to an estimated 10% 'take' of transferred input cells⁵¹.

Surface and intracellular antibody staining of mouse cells. Surface staining was performed for 30 min at 4 °C in PBS supplemented with 2% fetal calf serum (FACS buffer) with the following antibodies: CD4 (1:800, BD, clone GK1.5), CD8a (1:200, BD, clone 53-6.7), CD44 (1:200, BD, clone IM7), Ly5.1 (1:200, BD or BioLegend, clone A20), Ly5.2 (1:800, WEHI, clone 104), CX3CR1 (1:200, BioLegend, clone SA011F11), PD-1 (1:200, BioLegend, clone RMP1-30 or 29F.1A12), TIM-3 (1:200, BioLegend, clone RMT3-23), Ly108 (1:200, Thermo Fisher Scientific, clone eBio13G3-18D), CXCR5 (1:100, Thermo Fisher Scientific, clone SPRCL5), 2B4 (1:200, Thermo Fisher Scientific, clone eBio244F4), CD39 (1:200, Thermo Fisher Scientific, clone 24DMS1). LCMV-derived D^b/gp33-41 tetramers were obtained from the National Institutes of Health tetramer facility; tetramer staining was performed for 60 min at 4 °C in FACS buffer (1:100–1:400). Each cell-staining reaction was preceded by a 10-min incubation with purified anti-mouse CD16/32 antibody (1:1,000, FcgRIII block, Thermo Fisher Scientific, clone 2.4G2) and fixable viability dye (1:1,000, Thermo Fisher Scientific). For intracellular cytokine staining, splenocytes were ex vivo re-stimulated with gp33-41 (gp33) peptide (5 μM) for 5 h in the presence of Brefeldin A (Sigma) for the last 4.5 h, fixed and permeabilized using the Cytofix/Cytoperm (BD) or transcription factor-staining kit (eBioscience) and stained with anti-IFN-γ (1:400, Thermo Fisher Scientific, clone XMG1.2) and Granzyme B (1:200, Thermo Fisher Scientific, clone MHGB04). Intracellular transcription factor staining was performed with a transcription factor-staining kit (eBioscience) and the following antibodies: TCF1 (1:100, Cell Signaling, clone C63D9), TOX (1:100, Thermo Fisher Scientific, clone TXRX10) or green fluorescent protein (GFP; 1:30, BioLegend, clone FM264G). For GFP stain, cells were fixed with 4% formaldehyde before using the transcription factor-staining kit.

BACH2 overexpressing vector and retroviral transduction. The *Bach2* coding region was PCR amplified from mouse CD4⁺ T cell complementary DNA using BglII-flanked primers. The PCR product was digested with BglII and cloned into a BamHI-digested, calf intestinal alkaline phosphatase-treated pMSCV-Cherry plasmid. Recombinant plasmids were selected and orientation of the coding region was assessed by restriction digestion. The plasmid with the correct orientation was sequenced and used for further study.

Retroviral supernatant was produced from HEK293T human embryonic kidney cells transfected with retroviral expression pMSCV-plasmid containing either an mCherry or the Bach2-IRES-mCherry expression cassette. For retroviral transduction, P14 T cells were activated for approximately 40 h with

LCMV-derived gp33-41 peptide and interleukin-2 (50 U ml⁻¹). Activated P14 T cells were transduced via spin infection with viral supernatant supplemented with 50 μM 2-mercaptoethanol and 5 μg ml⁻¹ of polybrene for 90 min at 37 °C. P14 cells were subsequently incubated in RPMI medium at 37 °C for 1 h, after which interleukin-7 (10 ng ml⁻¹) was added. After 24 h, transduced cells were sort purified via Cherry expression and transferred into naive mice before LCMV infection.

RNA extraction, sequencing and analysis. RNA extraction from sorted P14 T cells was performed following the manufacturer's protocol using the RNeasy Plus Mini Kit (QIAGEN). Each sample group consisted of two experimental replicates. All samples were sequenced on an Illumina NextSeq 500 generating 75-bp paired-end reads. Reads were aligned to the mouse reference genome GRCm38/mm10 using the Subread aligner (v.1.6.2)⁵². Gene-level counts of the mapped reads were obtained using featureCounts (Rsubread v.1.34.6)^{53,54} and the inbuilt Rsubread annotation that is a modified version of the National Center for Biotechnology Information RefSeq mouse (mm10) genome annotation build 38.1. Genes that had a counts per minute (c.p.m.) <0.5 in all libraries were excluded from further analysis. Read counts were converted to log₂(counts per min), quantile normalized and precision weighted with the voom function of the limma package^{55,56}. A linear model was fitted to each gene, and empirical Bayes' moderated t-statistics were used to assess differences in expression⁵⁷. Genes were called differentially expressed if they achieved a false discovery rate (FDR) <0.1 and a fold-change >1. Gene set enrichment analysis was carried out using the Rotation Gene Set Test (ROAST) function implemented in the limma package⁵⁸. The barcode plot function in limma was used to plot the enrichment of the gene sets in a ranked gene list.

ATAC-seq and analysis. ATAC-seq was performed as described⁵⁹. Briefly, 35,000–50,000 sorted P14 cells were resuspended in 50 μl chilled ATAC lysis buffer (10 mM Tris-HCl, 10 mM NaCl, 3 mM MgCl₂, 0.1% (v:v) Igepal CA-630) and centrifuged for 10 min at 500g and 4 °C. Nuclei of an equivalent of 35,000 cells were resuspended in 35 μl of tagmentation buffer (2× Tagment DNA buffer, 20× Tagment DNA enzyme, Nextera library preparation kit) and incubated for 30 min at 37 °C. Next, tagmented DNA was isolated using the MinElute PCR purification kit (QIAGEN). Samples were PCR amplified with a common forward primer and unique barcoding reverse primers before tagmentation efficiency, and concentration was assessed with a bioanalyzer high-sensitivity DNA analysis kit (Agilent). Pooled libraries were cleaned from small (<150 bp) fragments and sequenced on a NextSeq 500 sequencer (Illumina) producing paired-end 75-bp reads. ATAC-seq data for naive T cells were downloaded from GEO with the accession code GSE86797 (ref. ³¹) and used as a control. Sequence reads were mapped to mouse genome GRCm38/mm10 using the Subread aligner. Only uniquely mapped reads were retained. ATAC peaks were called using Homer (v.4.10)⁶⁰ with an FDR cut-off of 1⁻⁵. Overlapping peaks from different samples were merged into a single peak region that covers all the overlapping peaks. Mapped reads were assigned to all the merged regions for each sample using featureCounts. Regions were removed from analysis if they failed to achieve a counts per minute value of ≥ 0.7 in at least one sample. Regions were annotated by assigning them to the nearest gene. Read counts for regions were converted to log₂(counts per min) and precision weighted with the limma voom function. A linear model was fitted to each region, and empirical Bayes-modulated t-statistics were used to assess differences in chromatin accessibility. An FDR cut-off of 0.1 was applied for calling differentially accessed regions. Motif enrichment of transcription factors in differentially accessible regions was performed using Homer with an FDR cut-off of 0.05.

Data analyses. Flow cytometry was performed using a BD Fortessa and sort purification was performed on a BD FACSaria Fusion. All data were analyzed using FlowJo v.10 (Tree Star). Graphs were prepared with Prism v.7 (GraphPad Software).

Reporting Summary. Further information on research design is available in the Nature Research Reporting Summary linked to this article.

Data availability

All data are available in the main text or the Extended Data materials. All materials used in the present study are available upon request from the lead authors. Sequencing data generated for this study have been deposited in the Gene Expression Omnibus database with accession code GSE142687.

References

45. Miyazaki, M. et al. The opposing roles of the transcription factor E2A and its antagonist Id3 that orchestrate and enforce the naive fate of T cells. *Nat. Immunol.* **12**, 992–1001 (2011).
46. Kometani, K. et al. Repression of the transcription factor Bach2 contributes to predisposition of IgG1 memory B cells toward plasma cell differentiation. *Immunity* **39**, 136–147 (2013).
47. Lee, P. P. et al. A critical role for Dnmt1 and DNA methylation in T cell development, function, and survival. *Immunity* **15**, 763–774 (2001).

48. Itoh-Nakadai, A. et al. The transcription repressors Bach2 and Bach1 promote B cell development by repressing the myeloid program. *Nat. Immunol.* **15**, 1171–1180 (2014).
49. Puglielli, M. T. et al. In vivo selection of a lymphocytic choriomeningitis virus variant that affects recognition of the GP33-43 epitope by H-2Db but not H-2K^b. *J. Virol.* **75**, 5099–5107 (2001).
50. Battegay, M. et al. Quantification of lymphocytic choriomeningitis virus with an immunological focus assay in 24- or 96-well plates. *J. Virol. Methods* **33**, 191–198 (1991).
51. Blattman, J. N. et al. Estimating the precursor frequency of naive antigen-specific CD8 T cells. *J. Exp. Med.* **195**, 657–664 (2002).
52. Liao, Y., Smyth, G. K. & Shi, W. The Subread aligner: fast, accurate and scalable read mapping by seed-and-vote. *Nucleic Acids Res.* **41**, e108 (2013).
53. Liao, Y., Smyth, G. K. & Shi, W. featureCounts: an efficient general purpose program for assigning sequence reads to genomic features. *Bioinformatics* **30**, 923–930 (2014).
54. Liao, Y., Smyth, G. K. & Shi, W. The R package Rsubread is easier, faster, cheaper and better for alignment and quantification of RNA sequencing reads. *Nucleic Acids Res.* **47**, e47 (2019).
55. Law, C. W., Chen, Y., Shi, W. & Smyth, G. K. voom: Precision weights unlock linear model analysis tools for RNA-seq read counts. *Genome Biol.* **15**, R29 (2014).
56. Ritchie, M. E. et al. limma powers differential expression analyses for RNA-sequencing and microarray studies. *Nucleic Acids Res.* **43**, e47 (2015).
57. McCarthy, D. J. & Smyth, G. K. Testing significance relative to a fold-change threshold is a TREAT. *Bioinformatics* **25**, 765–771 (2009).
58. Wu, D. et al. ROAST: rotation gene set tests for complex microarray experiments. *Bioinformatics* **26**, 2176–2182 (2010).
59. Buenrostro, J. D., Giresi, P. G., Zaba, L. C., Chang, H. Y. & Greenleaf, W. J. Transposition of native chromatin for fast and sensitive epigenomic profiling of open chromatin, DNA-binding proteins and nucleosome position. *Nat. Methods* **10**, 1213–1218 (2013).
60. Heinz, S. et al. Simple combinations of lineage-determining transcription factors prime *cis*-regulatory elements required for macrophage and B cell identities. *Mol. Cell* **38**, 576–589 (2010).

Acknowledgements

We thank T. Mason for technical support and T. Gebhardt, S. Nutt and members of the Kallies lab for discussions. This work was funded by the National Health and Medical Research Council (project grant no. 1085151 and Senior Research Fellowship no. 1139607 to A.K.), the Swiss National Science Foundation (fellowship nos. P300PA_177907 to D.T.U., P400PM_180807 to S.S.G. and P300PB_177934 to P.M.G.) and the Novartis Foundation for Medical–Biological Research (fellowship to S.S.G.). D.T.U. is a Special Fellow of the Leukemia and Lymphoma Society (fellowship no. 3387-19). W.S. is supported by a WEHI Centenary Fellowship funded by a donation from CSL Ltd. We acknowledge the Melbourne Cytometry Platform for provision of flow cytometry services.

Author contributions

D.T.U., S.S.G. and A.K. conceived the study, designed experiments, interpreted the results and wrote the manuscript. D.T.U. and S.S.G. performed the experiments with support from R.G. and P.M.G. A.V. generated the BACH2-overexpressing vector. D.C. and W.S. analyzed the sequencing data.

Competing interests

The authors declare no competing interests.

Additional information

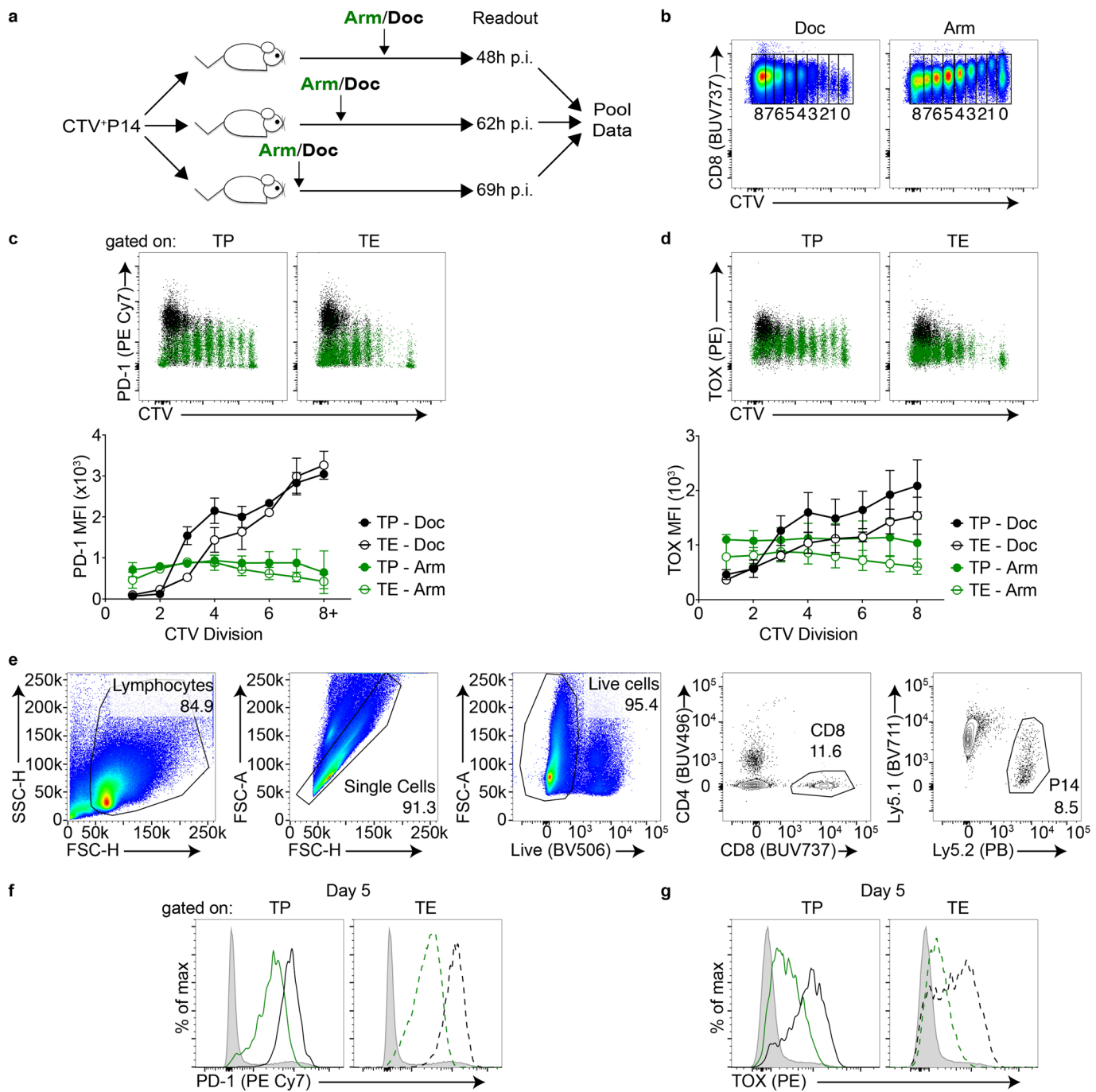
Extended data is available for this paper at <https://doi.org/10.1038/s41590-020-0760-z>.

Supplementary information is available for this paper at <https://doi.org/10.1038/s41590-020-0760-z>.

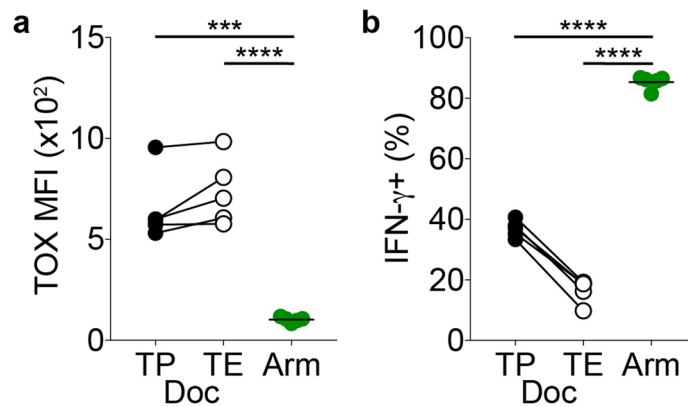
Correspondence and requests for materials should be addressed to D.T.U. or A.K.

Peer review information Peer reviewer reports available. Zoltan Fehervari was the primary editor on this article and managed its editorial process and peer review in collaboration with the rest of the editorial team.

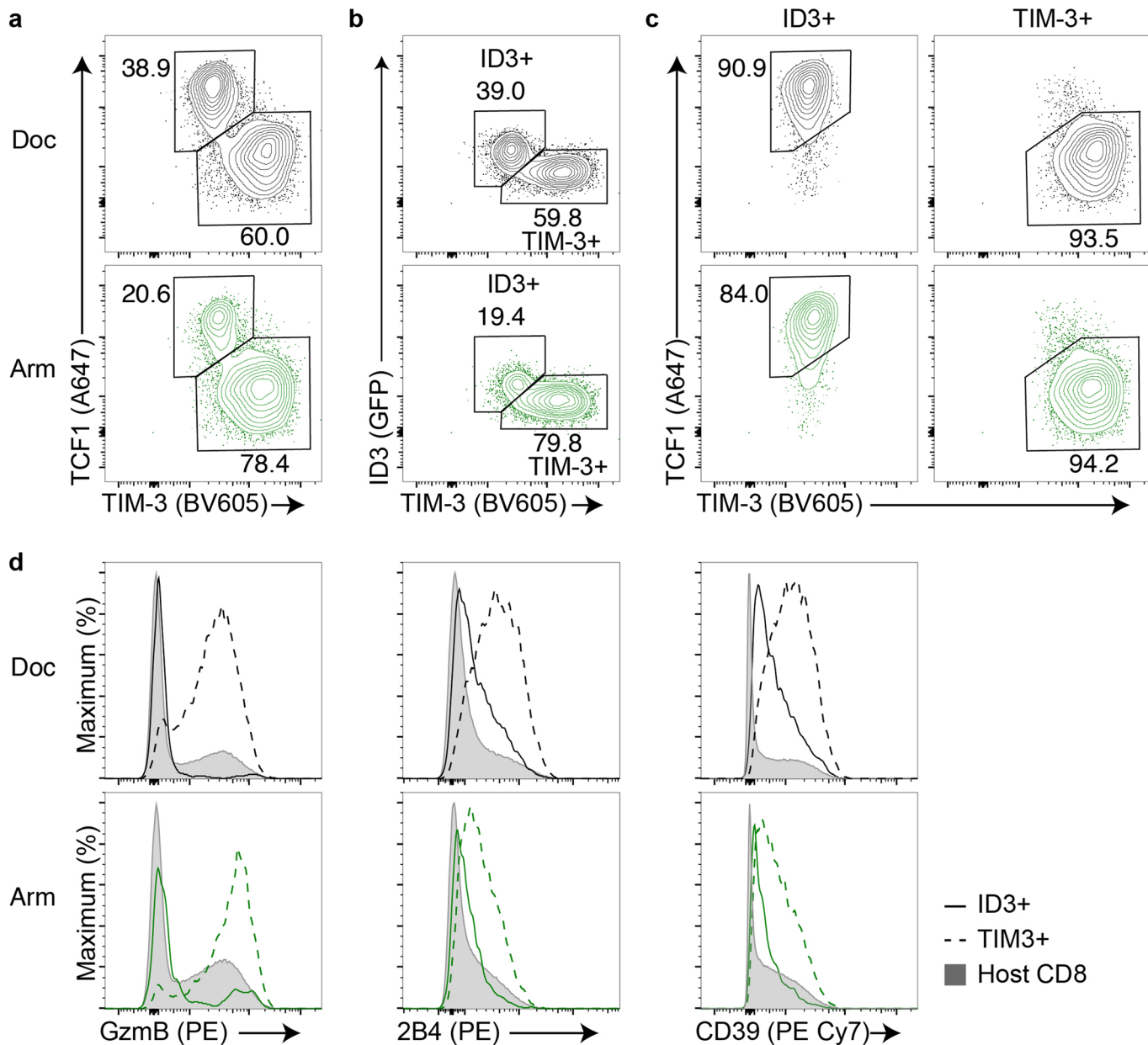
Reprints and permissions information is available at www.nature.com/reprints.



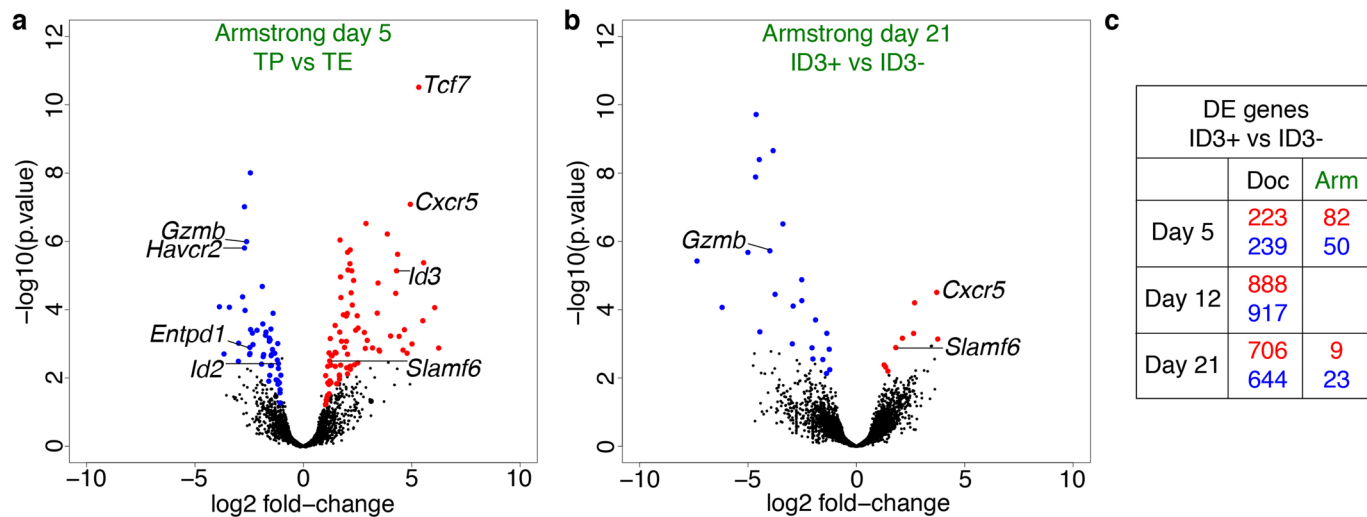
Extended Data Fig. 1 | High levels of antigen promote precursor T cell generation and PD-1 and TOX expression. **a**, Experimental scheme referring to **b-d** and Fig. 1a, b. Congenically marked P14 T cells were labelled with CellTrace Violet (CTV) and transferred into naïve mice, which were infected with either acute LCMV Armstrong (Arm) or chronic LCMV Docile (Doc). Spleens were analysed 48, 62 and 69 hours post infection (p.i.). For each experiment, all 12 biological replicates (four mice at 3 timepoints) were concatenated into one file in FlowJo. **b**, Representative FACS plots showing CTV-dilutions of P14 T cells from concatenated samples. **c, d**, Representative FACS plots showing PD-1 (**c**) and TOX expression (**d**) versus CTV-dilution (top). Samples from Docile infected mice are in black and from Armstrong in green. Mean fluorescent intensity (MFI) combined from two experiments (bottom). Data are representative of three individual experiments. Error bars indicate SEM. **e-g**, P14 T cells were transferred into congenically marked naïve recipient mice, which were infected with either LCMV Armstrong or Docile. **e**, Gating strategy for identification of P14 T cells. **f, g**, Representative histograms depicting PD-1 (**f**) and TOX (**g**) among TCF1⁺ precursor (TP, solid line, left) and TIM-3⁺ effector (TE, dashed line, right) P14 T cells on day 5 p.i. with high dose Docile (black) or Armstrong (green); grey represents host CD8⁺ T cells. Data are representative of at least three independent experiments with five mice per group.



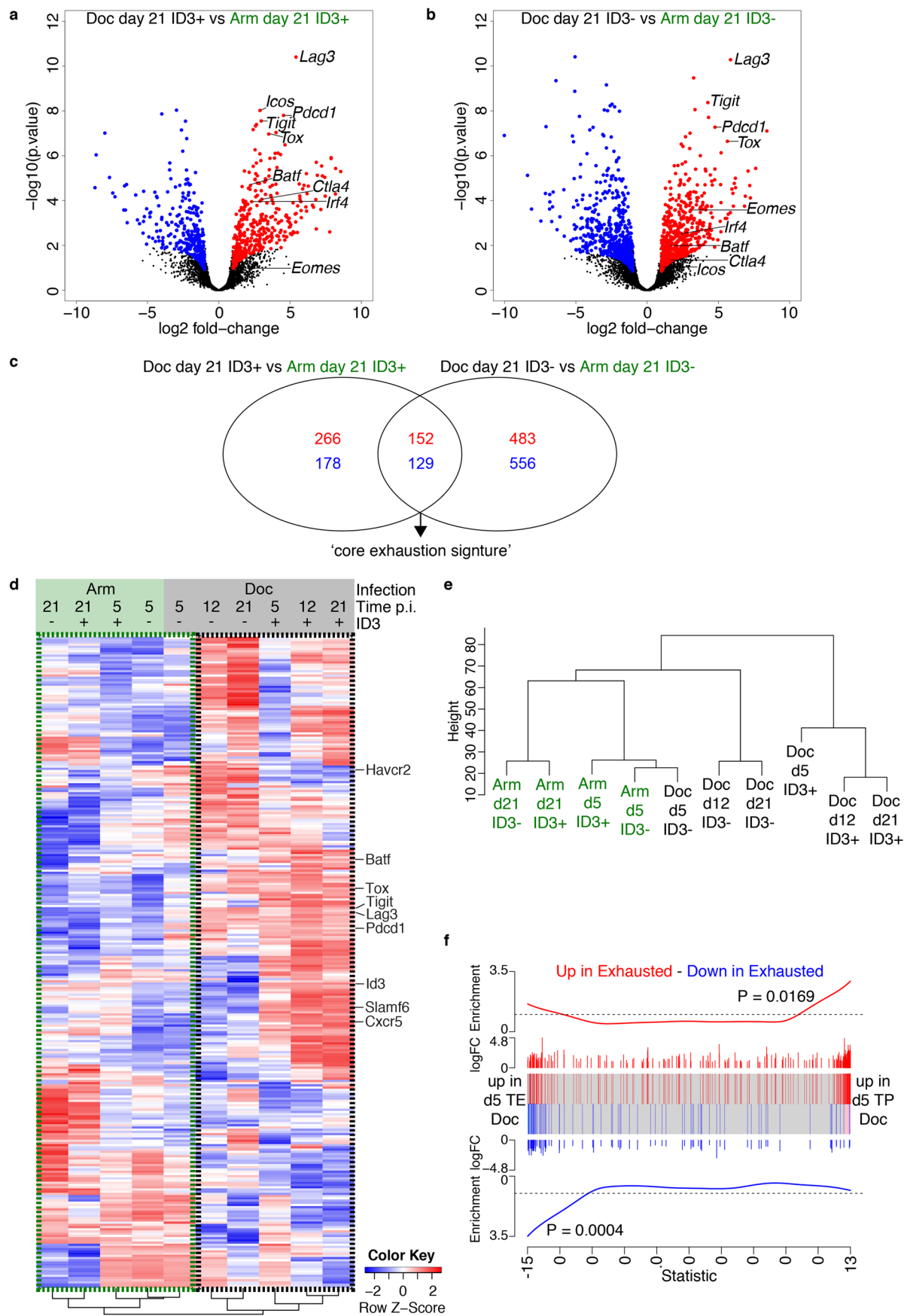
Extended Data Fig. 2 | Memory T cells in acutely-resolved infection express low levels of TOX and high amounts of IFN- γ . P14 T cells were transferred into congenically marked naïve recipient mice, which were infected with either LCMV Armstrong or Docile and analysed on day 21 p.i. **a**, TOX expression of TCF1⁺ precursor (TP, black solid dots) and TIM-3⁺ effector (TE, black open dots) P14 T cells from Docile compared to memory P14 T cells from Armstrong (green solid dots) infection. **b**, Frequencies of IFN- γ producing TP and TE P14 T cells from Docile compared to memory P14 T cells from Armstrong after ex vivo re-stimulation with LCMV-derived gp33 peptide. TP and TE cell segregation based on Ly108 and TIM-3 expression. Symbols represent individual mice; lines connect P14 T cells within the same host. Data are representative of at least three independent experiments with at least four mice per group. Statistical analysis was performed with unpaired Student's t test (two-tailed). ****p < 0.0001; ***p < 0.001.



Extended Data Fig. 3 | Phenotypic characterization of ID3⁺ and ID3⁻ T cells in chronic and acute infection. Congenically marked *Id3*^{GFP} P14 T cells were transferred into naïve mice, which were then infected with either LCMV Armstrong or Docile. **a**, TCF1 versus TIM-3 expression of P14 T cells from spleens on day 5 post LCMV Docile (top, black) or LCMV Armstrong (bottom, green) infection. **b**, ID3 versus TIM-3 expression of P14 T cells from spleens on day 5 post Docile or Armstrong infection. **c**, TCF1 versus TIM-3 expression of ID3⁺ TP and TIM-3⁺ TE cells from **b**. **d**, Expression of Granzyme B (GzmB), 2B4 and CD39 among ID3⁺TP and TIM-3⁺TE cells on day 5 post Docile or Armstrong infection. Histograms of ID3⁺TP cells in solid lines, ID3⁺TIM-3⁺ TE cells in dashed lines and host CD8⁺ T cells in grey are shown. Data are representative of at least two individual experiments with at least four mice each.

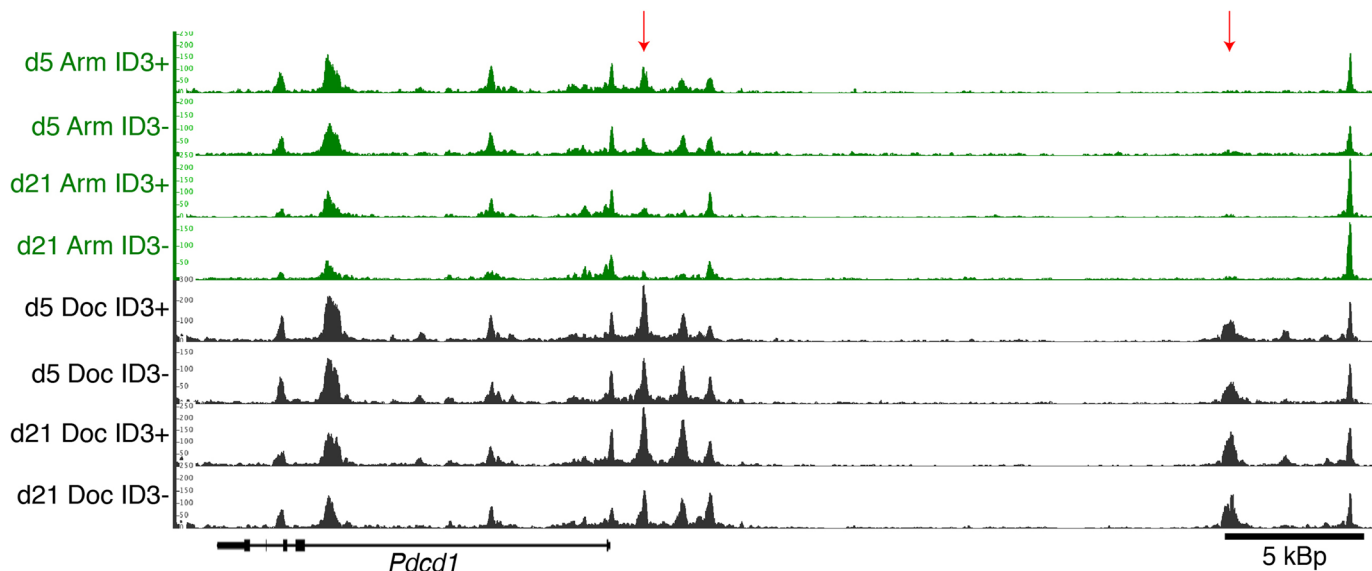


Extended Data Fig. 4 | Transcriptional differences between ID3⁺ and ID3⁻ P14 T cells in acute and chronic infection. Congenically marked *Id3*^{GFP} P14 T cells were transferred into naïve mice, which were then infected with either LCMV Armstrong or Docile. ID3⁺ and ID3⁻ P14 T cells from Armstrong infected mice were FACS purified for RNAseq analysis as described in Fig. 4. **a, b**, Volcano plots show differentially expressed (DE) genes between ID3⁺ and ID3⁻ P14 T cells obtained from Armstrong infected mice on day 5 p.i. (**a**) and day 21 p.i. (**b**). **c**, Number of DE genes in all comparisons including comparisons shown in Fig. 4a, b. Number of genes upregulated in ID3⁺ compared to ID3⁻ P14 T cells are indicated in red and genes downregulated in ID3⁺ P14 T cells are indicated in blue.

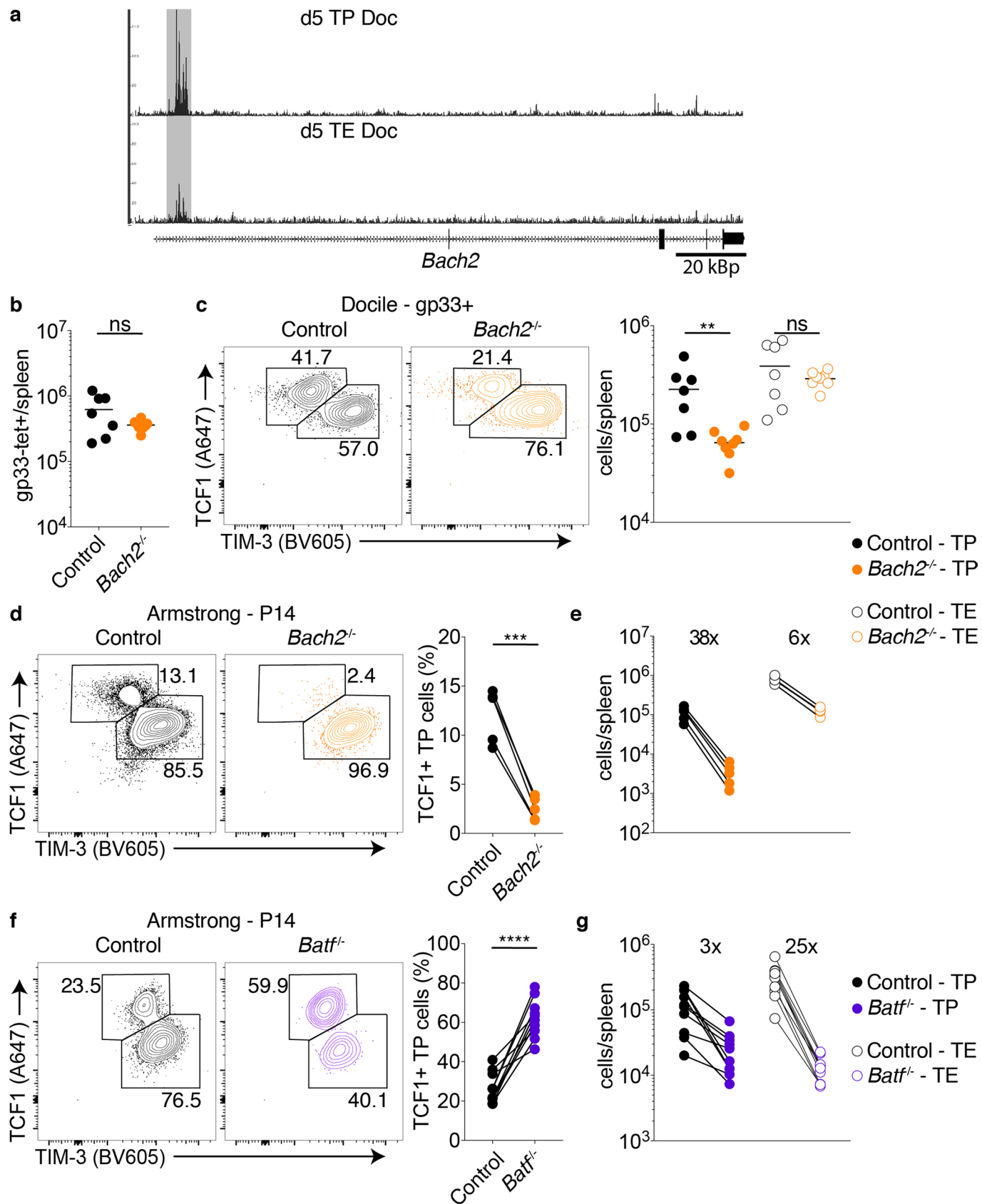


Extended Data Fig. 5 | See next page for caption.

Extended Data Fig. 5 | Generation of a core exhaustion T cell gene signature. Congenically marked *Id3^{GFP}* P14 T cells were transferred into naïve mice, which were infected with either LCMV Armstrong or Docile. ID3⁺ and ID3⁻ P14 T cells were FACS purified for RNAseq analysis as described in Fig. 4. **a, b**, Volcano plots show genes differentially expressed (DE) between ID3⁺ (**a**) and ID3⁻ (**b**) P14 T cells from day 21 Docile and Armstrong infections. **c**, Venn diagram shows numbers of DE genes common (core exhaustion signature) or unique to each comparison. Numbers in red highlight genes upregulated in Docile samples and numbers in blue genes downregulated in Docile. **d**, Heatmap established by unsupervised clustering of all generated samples based on the ‘dysfunctional vs polyfunctional’ signature defined by Alfei et al. 2019 (ref. ¹¹). Black (Docile) and green (Armstrong) boxes on top highlight origin of cells. Dotted squares highlight main two clusters; green square = polyfunctional phenotype, black square = exhausted phenotype. **e**, Hierarchical tree of unsupervised clustered heatmap. **f**, Gene set enrichment analysis of Docile derived day 5 TP versus TE cells using the ‘dysfunctional vs polyfunctional’ signature defined by Alfei et al. 2019 (ref. ¹¹). Barcode plots based on ROAST tests including p values from the tests are shown; signature genes upregulated are shown in red and genes downregulated in blue.

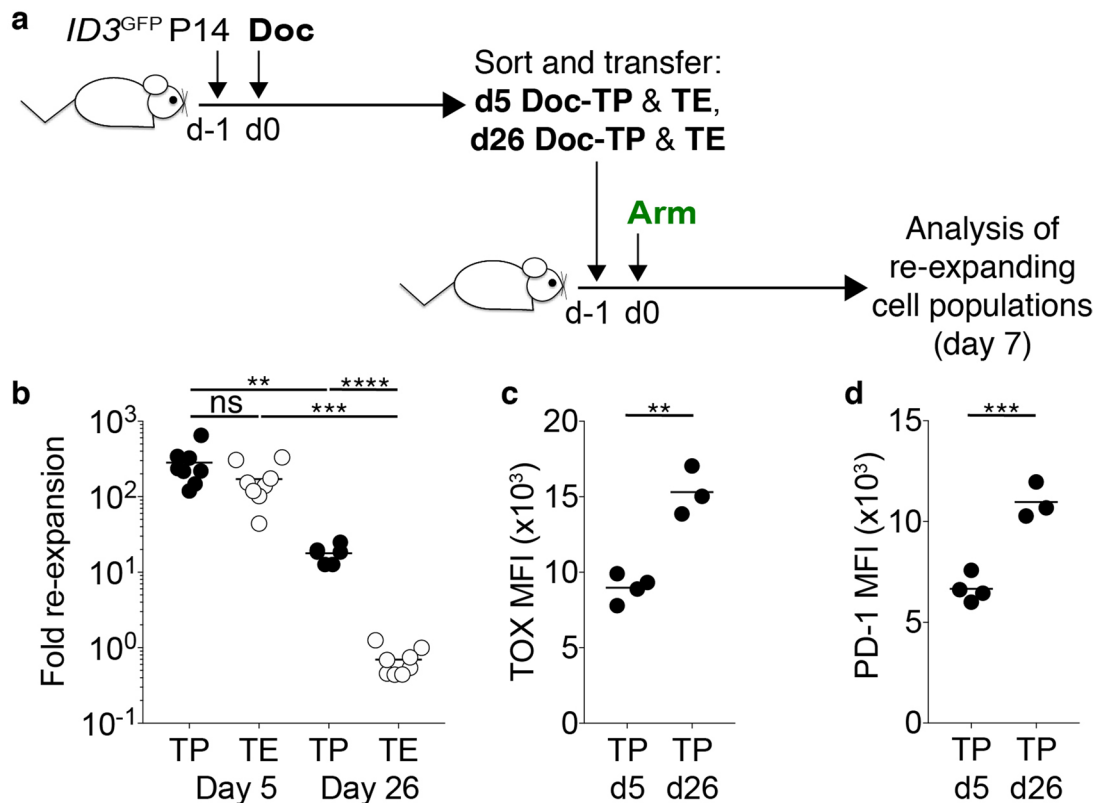


Extended Data Fig. 6 | The *Pdcd1* gene locus displays early enhanced accessibility in T cells responding to LCMV Docile infection. Congenically marked *Id3*^{GFP} P14 T cells were transferred into naïve mice, which were then infected with either LCMV Armstrong or Docile. ID3⁺ and ID3⁻ P14 T cells were FACS purified at days 5 and 21 p.i. and ATAC sequencing was performed. Chromatin accessibility of the *Pdcd1* locus is shown. Red arrows highlight regions that are differentially accessible between T cells obtained from Armstrong (green tracks) compared to Docile infected mice (black tracks). ATAC seq analysis was performed with two experimental replicates at each time point. Open chromatin tracks are based on merged replicates.



Extended Data Fig. 7 | See next page for caption.

Extended Data Fig. 7 | BACH2 and BATF regulate early precursor T cell differentiation. **a**, Congenically marked *Id3^{GFP}* P14 T cells were transferred into naïve recipient mice, which were then infected with LCMV Docile. 5 days p.i., ID3⁺ TP and ID3⁻ TE P14 T cells were purified and chromatin accessibility determined by ATAC sequencing. Chromatin accessibility of *Bach2* locus of TP and TE cells. Grey box highlights regions that are differentially accessible comparing the two samples. **b, c**, *Bach2^{fl/fl}Cd4^{Cre}* (*Bach2^{-/-}*) and *Cd4^{Cre}* (Control) mice were infected with Docile and analysed 5 days later. **b**, Absolute numbers of gp33-tetramer⁺CD8⁺ T cells. **c**, Plots show TCF1 and TIM-3 expression of gp33-tetramer⁺CD8⁺ T cells in *Bach2^{-/-}* and control mice (left), graph shows absolute numbers of TCF1⁺ TP and TIM-3⁺ TE cells among gp33-tetramer⁺CD8⁺ T cells in spleens (right). **d-g**, Congenically marked BACH2-deficient (*Bach2^{fl/fl}Cd4^{Cre}*, labelled as *Bach2^{-/-}*) and control P14 T cells (*Cd4^{Cre}*, labelled as control) (**b, c**) or *Batf^{-/-}* and *Batf^{+/+}* control P14 T cells (**d, e**) were co-transferred into naive mice, which were challenged with Armstrong and analysed 5 days later. **b, d**, TCF1 versus TIM-3 (left) and TCF1⁺ TP cell frequency (right) in spleens. **c, e**, Absolute numbers of TCF1⁺ TP and TIM-3⁺ TE cells. Numbers indicate fold increase in control compared to *Bach2^{-/-}* (**c**) or *Batf^{-/-}* cells (**d**). ATAC seq analysis was performed with two experimental replicates at each time point. Open chromatin tracks are based on merged replicates. Symbols in **b-e** represent individual mice; lines connect P14 T cells within the same host. Data are combined or representative of two independent experiments with at least three mice per group. Statistical analysis was performed with a paired Student's t test (two-tailed). ***p < 0.0001; ***p < 0.001; **p < 0.01; ns, not significant. MFI, mean fluorescent intensity. Error bars indicate SEM.



Extended Data Fig. 8 | Late precursor T cells retain higher levels of TOX and PD-1 after expansion in acute infection. **a**, Experimental scheme.

Congenically marked *Id3^{GFP}* P14 T cells were transferred into naïve mice, which were infected with LCMV Docile. 5 or 26 days p.i., ID3⁺TIM-3⁻ TP and ID3⁻TIM-3⁺ TE P14 T cells were FACS sorted and transferred into naïve mice, which were infected with Armstrong. Donor P14 T cells were analysed 7 days post infection. **b**, Fold expansion of donor T cell populations. **c**, **d**, MFI of TOX (**c**) and PD-1 (**d**) of donor P14 T cells. Symbols represent individual mice. Data are representative or combined of two experiments with at least 3 mice per group. Statistical analysis was unpaired Student's t test (two-tailed). ***p < 0.0001; **p < 0.001; **p < 0.01; ns, not significant.

Corresponding author(s): Axel Kallies

Last updated by author(s): Jun 24, 2020

Reporting Summary

Nature Research wishes to improve the reproducibility of the work that we publish. This form provides structure for consistency and transparency in reporting. For further information on Nature Research policies, see [Authors & Referees](#) and the [Editorial Policy Checklist](#).

Statistics

For all statistical analyses, confirm that the following items are present in the figure legend, table legend, main text, or Methods section.

n/a Confirmed

- The exact sample size (n) for each experimental group/condition, given as a discrete number and unit of measurement
- A statement on whether measurements were taken from distinct samples or whether the same sample was measured repeatedly
- The statistical test(s) used AND whether they are one- or two-sided
Only common tests should be described solely by name; describe more complex techniques in the Methods section.
- A description of all covariates tested
- A description of any assumptions or corrections, such as tests of normality and adjustment for multiple comparisons
- A full description of the statistical parameters including central tendency (e.g. means) or other basic estimates (e.g. regression coefficient) AND variation (e.g. standard deviation) or associated estimates of uncertainty (e.g. confidence intervals)
- For null hypothesis testing, the test statistic (e.g. F , t , r) with confidence intervals, effect sizes, degrees of freedom and P value noted
Give P values as exact values whenever suitable.
- For Bayesian analysis, information on the choice of priors and Markov chain Monte Carlo settings
- For hierarchical and complex designs, identification of the appropriate level for tests and full reporting of outcomes
- Estimates of effect sizes (e.g. Cohen's d , Pearson's r), indicating how they were calculated

Our web collection on [statistics for biologists](#) contains articles on many of the points above.

Software and code

Policy information about [availability of computer code](#)

Data collection

Flow cytometry was performed using a BD Fortessa and sort-purification was performed on a BD FACSaria Fusion. Samples were PCR-amplified with a common forward primer and unique barcoding reverse primers before tagmentation efficiency and concentration was assessed with a bioanalyzer high sensitivity DNA analysis kit (Agilent). Pooled libraries were cleaned from small (<150 bp) fragments and sequenced on a NextSeq 500 sequencer (Illumina) producing paired-end 75 bp reads.

Data analysis

All flow cytometry data were analysed using FlowJo 10 (Tree Star). Graphs were prepared and statistics calculated using Prism 7 (GraphPad Software). ATACseq track figures were generated using Integrated genome browser (version 9.1.4). For RNAseq analysis, gene-level counts of the mapped reads were obtained using featureCounts (Rsubread version 1.34.6) and the inbuilt Rsubread annotation that is a modified version of NCBI RefSeq mouse (mm10) genome annotation build 38.1.

For manuscripts utilizing custom algorithms or software that are central to the research but not yet described in published literature, software must be made available to editors/reviewers. We strongly encourage code deposition in a community repository (e.g. GitHub). See the Nature Research [guidelines for submitting code & software](#) for further information.

Data

Policy information about [availability of data](#)

All manuscripts must include a [data availability statement](#). This statement should provide the following information, where applicable:

- Accession codes, unique identifiers, or web links for publicly available datasets
- A list of figures that have associated raw data
- A description of any restrictions on data availability

All data are available in the main text or the supplementary materials. All materials used in this study are available upon request from the lead authors. Sequencing data generated for this study have been deposited in the Gene Expression Omnibus (GEO) database with accession number GSE142687.

Field-specific reporting

Please select the one below that is the best fit for your research. If you are not sure, read the appropriate sections before making your selection.

- Life sciences Behavioural & social sciences Ecological, evolutionary & environmental sciences

For a reference copy of the document with all sections, see nature.com/documents/nr-reporting-summary-flat.pdf

Life sciences study design

All studies must disclose on these points even when the disclosure is negative.

Sample size	Animal models used in this study are well established and yield low variance. Therefore, for each experiment, 3-5 animals and the experiment repeated with the same number of mice. Owing to low variance, statistical power was achieved with 3 mice the least. However, in most experiments many more mice were used.
Data exclusions	No data points were excluded
Replication	In vivo experiments were performed at least twice with minimum 3 mice per experiment. All replication attempts were successful. RNAseq and ATACseq - 2 replicates. Cells from 10-15 mice were pooled for each RNA and ATACseq sample.
Randomization	6-8 week old mice were randomly chosen and infected with either acute or chronic LCMV. This includes randomization based on sex as well as weight and exact age of mice.
Blinding	Acquisition of the data was done in a blinded manner.

Reporting for specific materials, systems and methods

We require information from authors about some types of materials, experimental systems and methods used in many studies. Here, indicate whether each material, system or method listed is relevant to your study. If you are not sure if a list item applies to your research, read the appropriate section before selecting a response.

Materials & experimental systems		Methods	
n/a	Involved in the study	n/a	Involved in the study
<input type="checkbox"/>	<input checked="" type="checkbox"/> Antibodies	<input checked="" type="checkbox"/>	<input type="checkbox"/> ChIP-seq
<input type="checkbox"/>	<input checked="" type="checkbox"/> Eukaryotic cell lines	<input type="checkbox"/>	<input checked="" type="checkbox"/> Flow cytometry
<input checked="" type="checkbox"/>	<input type="checkbox"/> Palaeontology	<input checked="" type="checkbox"/>	<input type="checkbox"/> MRI-based neuroimaging
<input type="checkbox"/>	<input checked="" type="checkbox"/> Animals and other organisms		
<input checked="" type="checkbox"/>	<input type="checkbox"/> Human research participants		
<input checked="" type="checkbox"/>	<input type="checkbox"/> Clinical data		

Antibodies

Antibodies used	BD: CD4 (GK1.5, Cat: 612952), CD8a (53-6.7, Cat: 612759), CD44 (IM7, Cat: 740215), Ly5.1 (A20, Cat: 558701, 553775) Biologend: Ly5.1 (A20, Cat: 110739), PD-1 (RMP1-30, Cat: 109110 or 29F.1A12, Cat: 135231), TIM3 (RMT3-23, Cat: 119721), CX3CR1 (SA011F11, Cat: 149031), GFP (FM264G, Cat: 338008) ThermoFisher: Ly108 (eBio13G3-19D, Cat: 17-1508-82), CXCR5 (SPRCL5, Cat: 46-7185-82), 2B4 (eBio244F4, Cat: 12-2441-82), CD39 (24DMS1, Cat: 25-0391-82), IFNg (XMG1.2, Cat: 25-7311-82), Granzyme B (GB12, Cat: MHGB04), TOX (TXRX10, , Cat: 12-6502-82 or 50-6502-82) Walter and Eliza Hall Institute: Ly5.2 (104), CD16/32 (2.4G2) NIH tetramer facility: LCMV-derived Db/gp33-41 tetramers Cell Signaling: TCF1 (C63D9, Cell Signaling)
Validation	all antibodies were titrated and validated using appropriate controls

Eukaryotic cell lines

Policy information about cell lines	
Cell line source(s)	Peter Doherty Institute
Authentication	not authenticated

Mycoplasma contamination

none

Commonly misidentified lines
(See [ICLAC](#) register)

N/A

Animals and other organisms

Policy information about [studies involving animals](#); [ARRIVE guidelines](#) recommended for reporting animal research

Laboratory animals

C57BL/6JArc (Ly5.1 or Ly5.2), Id3GFP, Bach2f/f, Cd4Cre, Bach2RFP, Batf-/-, P14Tg. All mice were 6-8 weeks of age when used. Males and Females were both used. Mice were housed under standard SPF conditions.

Wild animals

No wild animals were used in this project

Field-collected samples

None

Ethics oversight

University of Melbourne Animal Ethics Committee

Note that full information on the approval of the study protocol must also be provided in the manuscript.

Flow Cytometry

Plots

Confirm that:

- The axis labels state the marker and fluorochrome used (e.g. CD4-FITC).
- The axis scales are clearly visible. Include numbers along axes only for bottom left plot of group (a 'group' is an analysis of identical markers).
- All plots are contour plots with outliers or pseudocolor plots.
- A numerical value for number of cells or percentage (with statistics) is provided.

Methodology

Sample preparation

Single-cell splenocyte suspensions were obtained by mashing total spleens through a 70-um nylon cell strainer, and red blood cells were lysed with a hypotonic ammonium chloride-potassium bicarbonate buffer. Surface staining was performed for 30 min at 4 degrees. Each cell staining reaction was preceded by a 10-min incubation with purified anti-mouse CD16/32 Ab (FcgrII/III block; 2.4G2) and fixable viability dye. For intracellular cytokine staining, splenocytes were ex vivo re-stimulated with gp33-41 (gp33) peptide in the presence of Brefeldin A, fixed and permeabilized using the Cytofix/Cytoperm (BD) or transcription factor staining kit (eBioscience). Intracellular transcription factor staining was performed with a transcription factor staining kit (eBioscience). For GFP stain, cells were fixed with 4% formaldehyde prior using the transcription factor staining kit.

Instrument

Flow cytometry was performed using a BD Fortessa and sort-purification was performed on a BD FACSaria Fusion.

Software

All data were analysed using FlowJo 10 (Tree Star). Graphs were prepared with Prism 7 (GraphPad Software).

Cell population abundance

Cell populations analysed ranged from 500-10000 cells/mouse

Gating strategy

FSC-H/SSC-H was used to identify lymphocytes by size.

FSC-H/FSC-A was used to identify single cells.

FSC-A/viability to identify live cells.

CD4/CD8 to identify CD8+ T cells

Ly5.1/Ly5.2 was used to identify P14 T cells

Tick this box to confirm that a figure exemplifying the gating strategy is provided in the Supplementary Information.